Supersymmetry reach of Fermilab Tevatron upgrades: The large tan β case

Howard Baer
Department of Physics, Florida State University, Tallahassee, Florida 32306

Chih-Hao Chen
Department of Physics, University of California, Davis, California 95616

Manuel Drees
APCTP, 207-43 Cheongryangri-dong, Seoul 130-012, Korea

Frank Paige
Brookhaven National Laboratory, Upton, New York 11973

Xerxes Tata
Department of Physics and Astronomy, University of Hawaii, Honolulu, Hawaii 96822
(Received 26 February 1998; published 8 September 1998)

The Yukawa couplings of the tau lepton and the bottom quark become comparable to, or even exceed, electroweak gauge couplings for large values of the supersymmetry parameter tan β. As a result, the lightest tau slepton $\tilde{\tau}_1$ and bottom squark $\tilde{b}_1$ can be significantly lighter than corresponding sleptons and squarks of the first two generations. Gluino, chargino, and neutralino decays to third generation particles are significantly enhanced when tan β is large. This affects projections for collider experiment reach for supersymmetric particles. In this paper, we evaluate the reach of the Fermilab Tevatron $p\bar{p}$ collider for supersymmetric signals in the framework of the minimal supergravity model. We find that the reach via signatures with multiple isolated leptons (e and μ) is considerably reduced. For very large tan β, the greatest reach is attained in the multijet$+E_T^{\rm miss}$ signature. Some significant extra regions may be probed by requiring the presence of an identified b jet in jets$+E_T^{\rm miss}$ events, or by requiring one of the identified leptons in clean trilepton events to actually be a hadronic 1 or 3 charged prong tau. In an appendix, we present formulas for chargino, neutralino, and gluino three body decays which are valid at large tan β. [S0556-2821(98)02119-5]

PACS number(s): 14.80.Ly, 11.30.Pb, 13.85.Qk

I. INTRODUCTION AND MOTIVATION

The minimal supergravity (MSUGRA) model [1] is commonly regarded as the paradigm framework for phenomenological analyses of weak scale supersymmetry. The visible sector is taken to consist of the particles of the minimal supersymmetric standard model [2] (MSSM). One posits, in addition, the existence of ''hidden sector'' field(s), which couple to ordinary matter fields and their superpartners only via gravity. The conservation of R parity is assumed. Supersymmetry is broken in a hidden sector of the theory; supersymmetry breaking is then communicated to the visible sector via gravitational interactions. The technical assumption of minimality implies that kinetic terms for matter fields take the canonical form; this assumption, which is equivalent to assuming an approximate global U(n) symmetry between n chiral multiplets, leads to a common mass squared m_0^2 for all scalar fields, and a common trilinear term A_0 for all A parameters. These parameters, which determine the sparticle-particle mass splitting in the observable sector are taken to be comparable to the weak scale $M_{\rm weak}$. In addition, motivated by the apparently successful gauge coupling unification in the MSSM, one usually adopts a common value $m_{1/2}$ for all gaugino masses at the scale $M_{\rm GUT}\simeq 2\times 10^{16}$ GeV. For simplicity, it is commonly assumed that in fact the scalar masses and trilinear terms unify at $M_{\rm GUT}$ as well. The resulting effective theory, valid at energy scales $E<M_{\rm GUT}$, is then just the MSSM with the usual soft supersymmetry (SUSY) breaking terms, which in this case are unified at $M_{\rm GUT}$. The soft SUSY breaking scalar and gaugino masses, the trilinear A terms and in addition a bilinear soft term B, the gauge and Yukawa couplings and the supersymmetric μ term are all then evolved from $M_{\rm GUT}$ to some scale $M\simeq M_{\rm weak}$ using renormalization group equations (RGE's). The large top quark Yukawa coupling causes the squared mass of one of the Higgs fields to be driven negative, resulting in the breakdown of electroweak symmetry; this determines the value of μ^2. Finally, it is customary to trade the parameter B for tan β, the ratio of Higgs field vacuum expectation values. The resulting weak scale spectrum of superpartners and their couplings can thus be derived in terms of four continuous plus one discrete parameters

$$m_0,\ m_{1/2},\ A_0,\ \tan\beta,\ \text{and}\ \ \mathrm{sgn}(\mu), \tag{1.1}$$

in addition to the usual parameters of the standard model.

The consequences of the MSUGRA model have been investigated for collider experiments at the CERN LEP2 e^+e^- collider [3], the Fermilab Tevatron $p\bar{p}$ collider [4,5], the CERN Large Hadron Collider (LHC) pp collider [6] and a possible Next Linear e^+e^- Collider (NLC) operating at $\sqrt{s}\simeq 500$ GeV [7,8]. In all but the last of these studies (where

the effect of the tau Yukawa coupling on aspects of the phenomenology of the stau sector is carefully examined), small to moderate values of the parameter $\tan\beta \sim 2$–10 have been adopted. This was due in part to the fact that event generators such as ISAJET [9] had not been constructed to provide reliable calculations for large $\tan\beta$. In particular, effects of tau and bottom Yukawa couplings

$$f_b = \frac{g m_b}{\sqrt{2} M_W \cos\beta}, \quad f_\tau = \frac{g m_\tau}{\sqrt{2} M_W \cos\beta} \tag{1.2}$$

which become comparable to the electroweak gauge couplings and even to the top Yukawa coupling $f_t = g m_t/(\sqrt{2} M_W \sin\beta)$ if $\tan\beta$ is large, had not been completely included. The correct inclusion of these couplings has a significant impact [10,11] on the search for supersymmetry at colliders.

In the MSUGRA model, the parameter $\tan\beta$ can be as large as $\tan\beta \sim m_t/m_b$, where the quark masses are evaluated at a scale $\sim M_{\rm weak}$; since the running m_b is considerably smaller than 5 GeV, $\tan\beta$ values up to 45–50 are possible. Such large $\tan\beta$ values are indeed preferred in some SO(10) grand unified theory (GUT) models with Yukawa coupling unification. In practice, one finds that if $\tan\beta$ is chosen to be too large, f_b diverges before $M_{\rm GUT}$. A slightly stronger upper limit on $\tan\beta$ is obtained from the requirement that m_A^2, the mass of the pseudoscalar Higgs boson, should be positive. The precise value of the upper bound on $\tan\beta$ depends somewhat on the other MSUGRA parameters.

In a recent paper [11], we reported on an upgrade of the event generator ISAJET that correctly incorporated the effects of τ and b Yukawa interactions so that it would provide reliable predictions for supersymmetry with large $\tan\beta$. Novel phenomenological implications special to large values of $\tan\beta$ were pointed out: in particular, it was noted that while Tevatron signals in multilepton (e and μ) channels were greatly reduced, there could be new signals involving b jets and τ leptons via which to search for SUSY. In this paper, we focus our attention on the search for supersymmetry at the Main Injector (MI) upgrade of the Fermilab Tevatron $p\bar{p}$ collider ($\sqrt{s} = 2$ TeV, integrated luminosity $\int \mathcal{L} dt = 2\ {\rm fb}^{-1}$) and the proposed TeV33 upgrade ($\sqrt{s} = 2$ TeV, integrated luminosity $\int \mathcal{L} dt = 25\ {\rm fb}^{-1}$) for the case where $\tan\beta$ is large.

A. Sparticles masses at large $\tan\beta$

Large b and τ Yukawa couplings significantly alter the mass spectra of the sparticles and Higgs bosons as shown in Fig. 1. Here we plot various sparticle and Higgs boson masses versus $\tan\beta$ for MSUGRA parameters $m_{1/2} = 150$ GeV, $A_0 = 0$, and (a) $m_0 = 150$ GeV and (b) $m_0 = 500$ GeV, for both signs of μ. We fix the pole mass $m_t = 170$ GeV.

The b and τ Yukawa couplings contribute negatively to the renormalization group running of the sbottom and stau soft masses, driving them to lower values than soft masses for the corresponding first and second generation squarks and sleptons. In addition, the off-diagonal terms in the sbottom and stau mass-squared matrices $m_b(-A_b + \mu \tan\beta)$ and $m_\tau(-A_\tau + \mu \tan\beta)$ can result in significant mixing between left and right sbottom and stau gauge eigenstates, and a possible further decrease in the physical masses for the lighter of the two sbottom (and stau) mass eigenstates $m_{\tilde{b}_1}$ and $m_{\tilde{\tau}_1}$. If $\tan\beta$ is small, $\tilde{\tau}_1 \simeq \tilde{\tau}_R$, while (because of top quark Yukawa interactions) $\tilde{b}_1 \simeq \tilde{b}_L$. The impact of bottom and tau Yukawa interactions can be seen in Fig. 1: $m_{\tilde{\tau}_1} \simeq m_{\tilde{e}_R}$ at low $\tan\beta$, and as $\tan\beta$ increases, $m_{\tilde{\tau}_1}$ decreases, while $m_{\tilde{e}_R}$ remains constant. Likewise, $m_{\tilde{b}_1}$ decreases with increasing $\tan\beta$, while $m_{\tilde{d}_L}$ remains constant. In the case of frame (a), ultimately $m_{\tilde{b}_1}$ drops below $m_{\tilde{W}_1}$ and $m_{\tilde{Z}_2}$ so that the two body decays $\tilde{W}_1 \to \tilde{\tau}_1 \nu_\tau$ and $\tilde{Z}_2 \to \tilde{\tau}_1 \tau$ become allowed, and dominate the branching fractions.

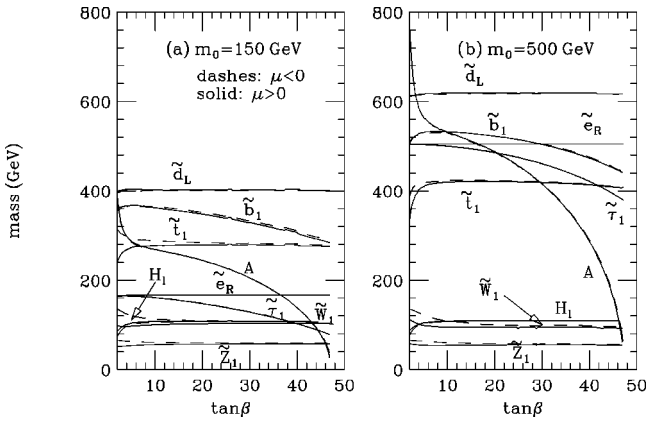

FIG. 1. Selected sparticle and Higgs boson masses versus $\tan\beta$ for the MSUGRA model for parameters (a) $(m_0, m_{1/2}, A_0) = (150,150,0)$ GeV and (b) $(m_0, m_{1/2}, A_0) = (150,500,0)$ GeV, for both signs of the parameter μ. We take $m_t = 170$ GeV.

It is well known that at low to moderate values of $\tan\beta$, the large top Yukawa coupling drives the Higgs mass $m_{H_2}^2$ to negative values, resulting in a breakdown of electroweak symmetry. At large $\tan\beta$, the large b and τ Yukawa couplings drive the other soft Higgs boson mass-squared $m_{H_1}^2$ to small or negative values as well. This results overall in a *decrease* in mass for the Higgs pseudoscalar m_A relative to its value at small $\tan\beta$. Since the values of the heavy scalar and charged Higgs boson masses are related to m_A, they decrease as well. This effect is also illustrated in Fig. 1, where the mass m_A decreases dramatically with increasing $\tan\beta$. The curves are terminated at the value of $\tan\beta$ beyond which $m_A^2 < 0$, and the correct pattern of electroweak symmetry breaking is not obtained as already mentioned. We found that the pseudoscalar mass m_A, obtained using the one-loop effective potential, is unstable by up to factors of 2 against scale variations for relatively low values of scale choice $Q \sim M_Z$. This instability would be presumably corrected by inclusion of two-loop corrections. We find the choice of scale $Q \sim \sqrt{m_{\tilde{t}_L} m_{\tilde{t}_R}}$ to empirically yield stable predictions of Higgs boson masses in the RG improved one-loop effective potential (where we include contributions from all third generation particles and sparticles). This scale choice effectively

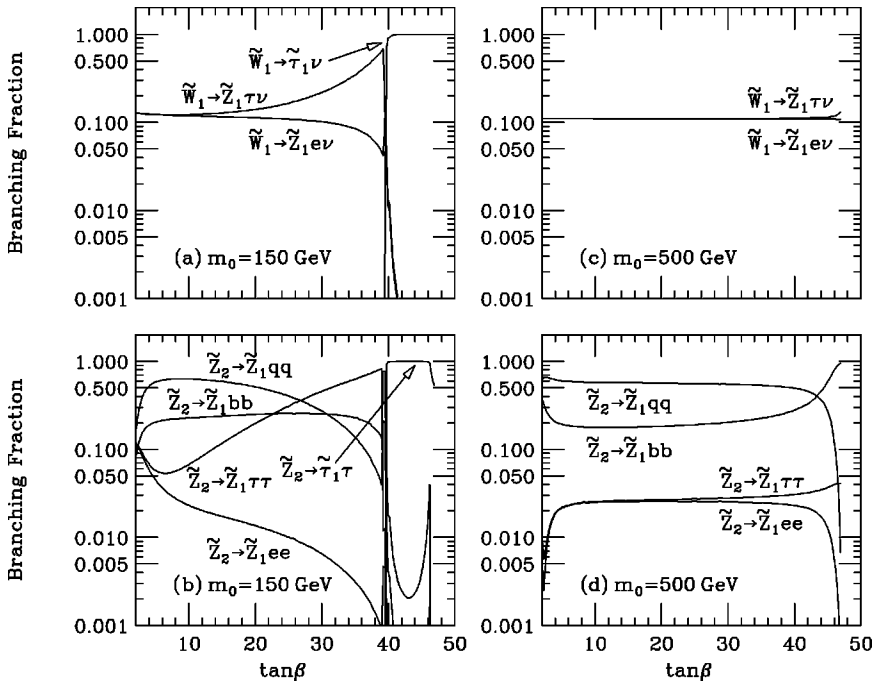

FIG. 2. Chargino ($\widetilde{W}_1$) and neutralino ($\widetilde{Z}_2$) branching fractions versus tan β. In (a) and (b), we take the parameters $(m_0, m_{1/2}, A_0) = (150,150,0)$ GeV while in (c) and (d) we take $(m_0, m_{1/2}, A_0) = (150,500,0)$ GeV. In all frames, $\mu > 0$ and $m_t = 170$ GeV. The discontinuities are an artifact of the narrow width approximation. In ISAJET, widths for three body and two-body decays are separately computed: the transition is, of course, smooth since the virtual particle smoothly goes on-shell.

includes some important two loop effects, and yields predictions for light scalar Higgs boson masses m_h in close accord with the results of Ref. [12].

B. Sparticle decays at large tan β

For large values of tan β, b and τ Yukawa couplings become comparable in strength to the usual gauge interactions, so that Yukawa interaction contributions to sparticle decay rates are non-negligible and can even dominate. This could manifest itself as lepton nonuniversality in SUSY events. Also, because of the reduction of masses referred to above, chargino and neutralino decays to stau, sbottom and various Higgs bosons may be allowed, even if the corresponding decays would be kinematically forbidden for small tan β values. The reduced stau, sbottom, and Higgs boson masses can also increase sparticle branching ratios to third generation particles via virtual effects. These enhanced decays to third generation particles can radically alter the expected SUSY signatures at colliders.

We have recalculated the branching fractions for the $\widetilde{g}$, $\widetilde{b}_i$, $\widetilde{t}_i$, $\widetilde{\tau}_i$, $\widetilde{\nu}_\tau$, $\widetilde{W}_i$, $\widetilde{Z}_i$, h, H, A, and $H^\pm$ particles and sparticles including sbottom and stau mixing as well as effects of b and τ Yukawa interactions. For Higgs boson decays, we use the formulas in Ref. [13]. We have recalculated the decay widths for $\widetilde{g}\to tb\widetilde{W}_i$ and $\widetilde{g}\to bb\widetilde{Z}_i$. These have been calculated previously by Bartl *et al.* [14]; our results agree with theirs if we use pole fermion masses to calculate the Yukawa couplings. In ISAJET, we use the running Yukawa couplings evaluated at the scale $Q = m_{\widetilde{g}}$ (m_t) to compute decay rates for the gluino ($\widetilde{W}_i, \widetilde{Z}_i$). This seems a more appropriate choice, and it significantly alters the decay widths when effects of f_b are important. The $\widetilde{Z}_i\to\tau\overline{\tau}\widetilde{Z}_j$ and $\widetilde{Z}_i\to b\overline{b}\widetilde{Z}_j$ decays take place via eight diagrams ($\widetilde{f}_{1,2}$, $\overline{\widetilde{f}}_{1,2}$, Z, h, H, and A exchanges). In our calculation of $\widetilde{g}$ and $\widetilde{Z}_i$ decays, we have neglected b and τ masses except in the Yukawa couplings and in the phase space integration. We have also computed the widths for decays $\widetilde{W}_i\to\widetilde{Z}_j\tau\nu$ which are mediated by W, $\widetilde{\tau}_{1,2}$, $\widetilde{\nu}_\tau$ and $H^\pm$ exchanges; in these cases, we retain m_τ effects only in the Yukawa couplings. Formulas for these three-body decays are presented in the Appendix.

To illustrate the importance of the Yukawa coupling effects, we show selected branching ratios of $\widetilde{W}_1$ and $\widetilde{Z}_2$ in Fig. 2. In all frames we take $\mu > 0$. Frames (a) and (b) are for the MSUGRA case $(m_0, m_{1/2}, A_0) = (150,150,0)$ GeV; frames (c) and (d) show the same branching fractions, but take $m_0 = 500$ GeV instead. In frame (a), for low tan β we see that the $\widetilde{W}_1\to e\nu\widetilde{Z}_1$ and $\widetilde{W}_1\to\tau\nu\widetilde{Z}_1$ branching ratios are very close in magnitude, reflecting the smallness of f_τ. For tan $\beta \gtrsim 10$, these branchings begin to diverge, with the branching to τ's becoming increasingly dominant. For tan $\beta > 40$, the two body mode $\widetilde{W}_1\to\widetilde{\tau}_1\nu$ opens up and quickly dominates. Since this decay is followed by $\widetilde{\tau}_1\to\tau\widetilde{Z}_1$, the end products of chargino decays here are almost exclusively tau leptons plus missing energy.

In frame (b), we see at low tan β the $\widetilde{Z}_2\to ee\widetilde{Z}_1$ and $\widetilde{Z}_2\to\tau\overline{\tau}\widetilde{Z}_1$ branchings are large ($\sim$10%) and equal, again because of the smallness of the Yukawa coupling. Except for parameter regions where the leptonic decays of $\widetilde{Z}_2$ are

strongly suppressed, $\tilde{W}_1\tilde{Z}_2$ production leads to the well known $3l(=e,\mu)$ signature for the Tevatron collider [15]. As $\tan\beta$ increases beyond about 5, these branchings again diverge, and increasingly $\tilde{Z}_2\to\tau\bar{\tau}\tilde{Z}_1$ dominates. Results of phenomenological analyses of trilepton signals for $\tan\beta$ $\sim$8–10 obtained using older versions of ISAJET should, therefore, be interpreted with caution. For $\tan\beta>40$, $\tilde{Z}_2\to\tau\tilde{\tau}_1$ opens up, and becomes quickly close to 100%. Near the edge of parameter space ($\tan\beta\sim45$), the $\tilde{Z}_2\to\tilde{Z}_1h$ decay opens up, resulting in a reduction of the $\tilde{Z}_2\to\tau\tilde{\tau}_1$ branching fraction.

In frame (c), the large value of $m_0=500$ GeV yields a large value of $m_{\tilde{\tau}_1}$ (and other slepton masses) even if $\tan\beta$ is large. In this case, the $\tilde{W}_1$ branching fractions are dominated by the virtual W boson, so that $B(\tilde{W}_1\to\tilde{Z}_1e\nu)$ and $B(\tilde{W}_1\to\tilde{Z}_1\tau\nu)$ are nearly equal over almost the entire range of $\tan\beta$. The branching fractions of $\tilde{Z}_2$ for $m_0=500$ GeV are shown in frame (d). As in frame (c), the branching fraction of $\tilde{Z}_2$ to τ's and e's is nearly the same except when $\tan\beta\geqslant35-40$. In this case, there is a steadily increasing branching fraction of $\tilde{Z}_2\to\tilde{Z}_1b\bar{b}$ (and to some extent, also of $\tilde{Z}_2\to\tilde{Z}_1\tau\bar{\tau}$), which is mainly a reflection of the increasing importance of virtual Higgs bosons in the $\tilde{Z}_2$ three-body decays. We mention that for values of $\tan\beta$ somewhat below the range where the decay $\tilde{Z}_2\to\tilde{Z}_1h$ becomes kinematically allowed, contributions from *all* neutral Higgs bosons are important.

The above considerations motivated us to begin a systematic exploration of how signals for supersymmetry may be altered if $\tan\beta$ indeed turns out to be very large. To facilitate this analysis, we have incorporated the above calculations into the computer program ISAJET 7.32, so that realistic simulations of sparticle production and decay can be made for large $\tan\beta$.

Another important effect at large $\tan\beta$ is that tau Yukawa interactions can alter the mean polarization of the τ's produced in chargino and neutralino decays. This, in turn, alters the energy distribution of the visible decay products of the τ. The τ polarization information is saved in ISAJET and used to dictate the energy distribution of the τ decay products.

The rest of this paper is organized as follows. In Sec. II, we describe aspects of our event generation and analysis program for Tevatron experiments, including a catalog of some of the possible signals for supersymmetry at large $\tan\beta$. In Sec. III, we present numerical results of our generation of supersymmetric signals and SM backgrounds, and show the reach of the Tevatron MI and TeV33 in the parameter space of the MSUGRA model. In Sec. IV, we present a summary and conclusions from our work. Some lengthy three-body decay formulas are included in the Appendix.

II. EVENT SIMULATION, SIGNATURES, AND CUTS

In several previous works [4], a variety of signal channels for the discovery of supersymmetry at the Tevatron were investigated, and plots were shown for the reach of the Tevatron MI and TeV33 in the parameter space of the MSUGRA model. The simulation of SUSY signal events was restricted to parameter space values of $\tan\beta=2$ and 10. The promising discovery channels that were investigated included the following: multijet$+E_T^{\rm miss}$ events (veto hard, isolated leptons) (J0L); events with a single isolated lepton plus jets$+E_T^{\rm miss}$ (J1L); events with two opposite sign isolated leptons plus jets$+E_T^{\rm miss}$ (JOS); events with two same sign isolated leptons plus jets$+E_T^{\rm miss}$ (JSS); events with three isolated leptons plus jets$+E_T^{\rm miss}$ (J3L); events with two isolated leptons$+E_T^{\rm miss}$ (no jets, clean) (COS); events with three isolated leptons$+E_T^{\rm miss}$ (no jets, clean) (C3L). In these samples, the number of leptons is *exactly* that indicated, so that these samples are nonoverlapping. For Tevatron data samples on the order of 0.1 fb^{-1}, the J0L signal generally gave the best reach for supersymmetry. It is the classic signature for detecting gluinos and squarks at hadron colliders. For larger data samples typical of those expected at the MI or TeV33, the C3L signal usually gave the best reach. In the present paper, we will extend these results to the large $\tan\beta$ region of MSUGRA parameter space; we will also look for new signatures which may be indicative of supersymmetry at large $\tan\beta$.

By examining the branching fractions in Fig. 2, we expect in general at large $\tan\beta$ that there would be a reduction in supersymmetric events containing isolated e's or μ's. We also expect for large $\tan\beta$ and small m_0 a more conspicuous presence of isolated τ leptons (defined by hadronic one- or three-charged prong jets as discussed below). For large $\tan\beta$ and large m_0, we expect an increased presence of tagged b jets (defined by displaced decay vertices or by identification of a muon inside of a jet). For these reasons, we have expanded the set of event topologies via which to search for SUSY to include, in addition: multijet$+E_T^{\rm miss}$ events which include at least one tagged b jet (J0LB); multijet$+E_T^{\rm miss}$ events which include at least one tagged τ jet (J0LT); multijet$+E_T^{\rm miss}$ events which include at least either a tagged b jet or a tagged τ jet (J0LBT); opposite-sign isolated dilepton plus jet$+E_T^{\rm miss}$ events where at least one of the isolated leptons is actually a tagged τ jet (JOST); same-sign isolated dilepton plus jet$+E_T^{\rm miss}$ events where at least one of the isolated leptons is actually a tagged τ jet (JSST); isolated trilepton plus jet$+E_T^{\rm miss}$ events where at least one of the isolated leptons is actually a tagged τ jet (J3LT); clean opposite-sign isolated dilepton$+E_T^{\rm miss}$ events where at least one of the isolated leptons is actually a tagged τ jet (COST); clean isolated trilepton$+E_T^{\rm miss}$ events where at least one of the isolated leptons is actually a tagged τ jet (C3LT). We note that some of these event samples are no longer nonoverlapping; for instance, the J0LB sample is a subset of the canonical $E_T^{\rm miss}$ (J0L) sample. In the tau samples, the lepton multiplicity is again exactly that indicated, except that at least one of the leptons is required to be identified as a τ.

To model the experimental conditions at the Tevatron, we use the toy calorimeter simulation package ISAPLT. We simulate calorimetry covering $-4<\eta<4$ with cell size $\Delta\eta\times\Delta\phi=0.1\times0.0875$. We take the hadronic (electromagnetic) energy resolution to be $70\%/\sqrt{E}$ ($15\%/\sqrt{E}$). Jets are defined as hadronic clusters with $E_T>15$ GeV within a cone with

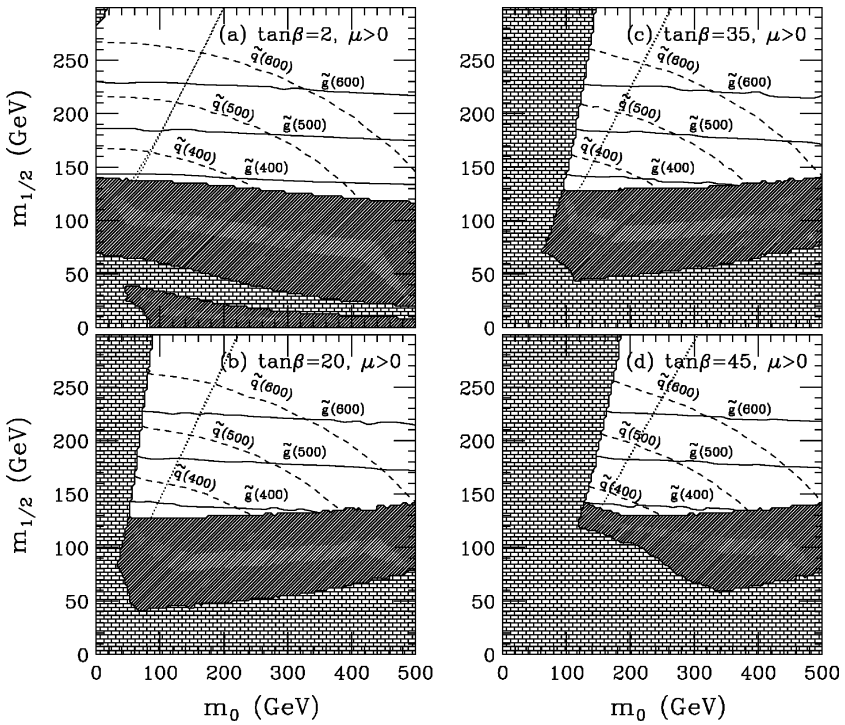

FIG. 3. Gluino and squark mass contours in the m_0 vs $m_{1/2}$ parameter plane, for (a) tan β=2, (b) tan β=20, (c) tan β=35, and (d) tan β=45. In all frames, we take $A_0=0$, $\mu>0$, and $m_t=170$ GeV. The bricked regions are excluded by theoretical constraints, while the gray regions are excluded by LEP2 bounds on $m_{\tilde{W}_1}$.

$\Delta R=\sqrt{\Delta\eta^2+\Delta\phi^2}=0.7$. We require that $|\eta_j|\leqslant 3.5$. Muons and electrons are classified as isolated if they have $p_T>5$ GeV, $|\eta(l)|<2.5$, and the visible activity within a cone of $R=0.3$ about the lepton direction is less than $\max[E_T(l)/4,2\text{ GeV}]$. For tagged b jets, we require a jet (using the above jet requirement) to have in addition $|\eta_j|<2$ and to contain a b hadron. Then the jet is identified as a b jet with a 50% efficiency. To identify a τ jet, we require a jet with just 1 or 3 charged prongs with $p_T>1$ GeV within 10° of the jet axis, and no other charged prongs within 30° of the jet axis. The invariant mass of the three prong jets must be less than m_τ, and the net charge of the three prongs should be ± 1. QCD jets with $p_T=15\,(\geqslant 50)$ GeV are misidentified as τ jets with a probability [16] of 0.5% (0.1%), with a linear interpolation in between. In our analysis, we neglect multiple scattering effects, nonphysics backgrounds from photon or jet misidentification, and make no attempt to explicitly simulate any particular detector.

We incorporate in our analysis the following trigger conditions: (1) one isolated lepton with $p_T(l)>15$ GeV and $E_T^{\rm miss}>15$ GeV; (2) $E_T^{\rm miss}>35$ GeV; (3) two isolated leptons each with $E_T>10$ GeV and $E_T^{\rm miss}>10$ GeV; (4) one isolated lepton with $E_T>10$ GeV plus at least one jet plus $E_T^{\rm miss}>15$ GeV; (5) at least four jets per event, each with $E_T>15$ GeV. Thus, every signal or background event must satisfy at least one of the above conditions.

We have generated the following physics background processes using ISAJET: $t\bar{t}$ production, $W+$jets, $Z+$jets, WW, WZ, and ZZ production and QCD (mainly from $b\bar{b}$ and $c\bar{c}$ production). Each background subprocess was generated with subprocess final state particles in p_T bins of 25–50 GeV, 50–100 GeV, 100–200 GeV, 200–400 GeV, and 400–600 GeV.

III. THE REACH OF THE FERMILAB TEVATRON FOR MSUGRA

We present our main results for the reach of the Tevatron for MSUGRA at large tan β in the m_0 vs $m_{1/2}$ parameter space plane for $A_0=0$ and for tan β=2, 20, 35, and 45. Our results are shown for $\mu>0$ only. For small tan $\beta\sim 2$, the $\mu<0$ results differ substantially from the $\mu>0$ results, and are shown in Ref. [4]. As tan β increases, the positive and negative μ results become increasingly indistinguishable.

In Fig. 3 we show for orientation contours of constant $m_{\tilde{g}}$ and $m_{\tilde{q}}$ in the m_0 vs $m_{1/2}$ plane. The bricked regions are excluded by either lack of appropriate electroweak symmetry breaking, or due to the $\tilde{\tau}_1$ or $\tilde{W}_1$ being the LSP instead of the $\tilde{Z}_1$. The gray regions are excluded by previous experimental sparticle searches, and the excluded region [3] is dominantly formed by the LEP2 bound that $m_{\tilde{W}_1}>80$ GeV [17]. The most noticeable feature of Fig. 3 is that the theoretically excluded region increases significantly as tan β increases. In the low m_0 region, this is due to the decrease in $\tilde{\tau}_1$ mass, making it become the LSP. The contours of $m_{\tilde{g}}$ and $m_{\tilde{q}}$ on the other hand are relatively constant and change little with tan β. The region to the left of the dotted lines denotes where the decay modes $\tilde{W}_1\to\tilde{\tau}_1\nu$ and $\tilde{Z}_2\to\tilde{\tau}_1\tau$ become accessible.

As in our previous analysis of signals at low tan β [4], for channels involving jets, we require of all signals, jet multi-

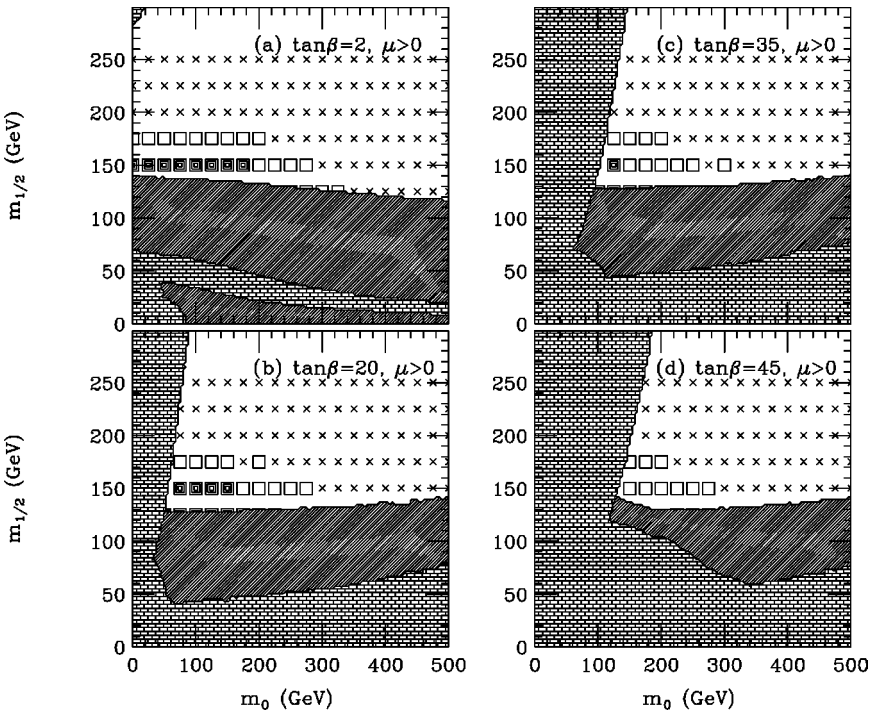

FIG. 4. A plot of points accessible to Tevatron MI and TeV33 searches for MSUGRA via $E_T^{\rm miss}+$ multijet events. A 5σ signal above background is found for some value of E_T^c for the MI for gray squares, while white squares are accessible only at TeV33. Points with crosses are inaccessible to MI and TeV33.

plicity, $n_{\rm jets}-n_{\tau-{\rm jets}}\geqslant 2$; $E_T^{\rm miss}>40$ GeV; and $E_T(j_1)$, $E_T(j_2)>E_T^c$, and $E_T^{\rm miss}>E_T^c$, where the parameter E_T^c is taken to be $E_T^c=15$, 40, 60, 80, 100, 120, 140, 160 GeV. This requirement serves to give some optimization of cuts for different masses of SUSY particles.

We generate signal events for each point on a 25 GeV$\times$25 GeV grid in the $m_0-m_{1/2}$ plane. For an observable signal, we require at least five signal events after all cuts (including those detailed below) are imposed, with $N_{\rm signal}$ exceeding $5\sqrt{N_{\rm background}}$. Any signal is considered observable if it meets the observability criteria for at least *one* of the values of E_T^c. In addition, we require the ratio of signal and background to exceed 0.2 for all luminosities.

A. Reach via the J0L channel

As in Ref. [4], for multijet$+E_T^{\rm miss}$ events (J0L), we require in addition to the above transverse sphericity $S_T>0.2$ and $\Delta\phi(\overrightarrow{E_T^{\rm miss}},\overrightarrow{E_{T_j}})>30°$. In Fig. 4, we show the Tevatron reach via the J0L channel. We found no parameter space points accessible to Tevatron experiments with 0.1 fb^{-1} of integrated luminosity (approximately the run I data sample) in this or any other channel; points denoted by gray squares are accessible with 2 fb^{-1} while those with open squares are accessible with 25 fb^{-1}. Points denoted by crosses are not visible at any of the luminosity upgrade options considered. In frame (a), no black squares are visible; regions normally accessible to Tevatron experiments with just 0.1 fb^{-1} of integrated luminosity have been excluded by the negative results of LEP2 searches for charginos. This is strictly valid only within the model framework, and should not be regarded as a direct bound on $m_{\tilde g}$. Regardless of the LEP2 bounds, Tevatron experiments should directly probe this region via the independent search for strongly interacting sparticles. Note that even within the MSUGRA framework, for $\mu<0$ and tan $\beta=2$, where $m_{\tilde W_1}$ is considerable heavier for the same $m_{1/2}$ values, there still exist parameter space points accessible with only 0.1 fb^{-1} [4]. A significant number of gray squares appear in frame (a), denoting regions with $m_{\tilde g}\sim 400$ GeV that can be probed at the MI. As tan β increases, the theoretically excluded region absorbs some of these points at low m_0, while some of the high m_0 points become inaccessible. In the latter case, much of the signal actually comes from $\tilde W_1\overline{\tilde W_1}$ and $\tilde W_1\tilde Z_2$ production, and these particles decay decreasingly into jetty final states, so the J0L signal diminishes. Finally, for very large tan $\beta=45$, none of the parameter space in this channel is open to MI searches. For TeV33, we see that $m_{1/2}\sim 175$ GeV ($m_{\tilde g}\sim 475$ GeV) can be probed in all of the frames (a)–(d) as long as m_0 is not much larger. The largest reach occurs when E_T^c attains its largest value of $E_T^c=160$ GeV.

B. Reach via the J0LB channel

In Fig. 5, we show the reach in the $E_T^{\rm miss}+$jets channel, where in addition we require at least one tagged *b* jet (J0LB). Comparing with Fig. 4, we see that the requirement of a tagged *b* jet considerably reduces the reach of the MI. Furthermore, the parameter space points with $m_{1/2}=175$ GeV are no longer accessible to TeV33. In other words, a higher

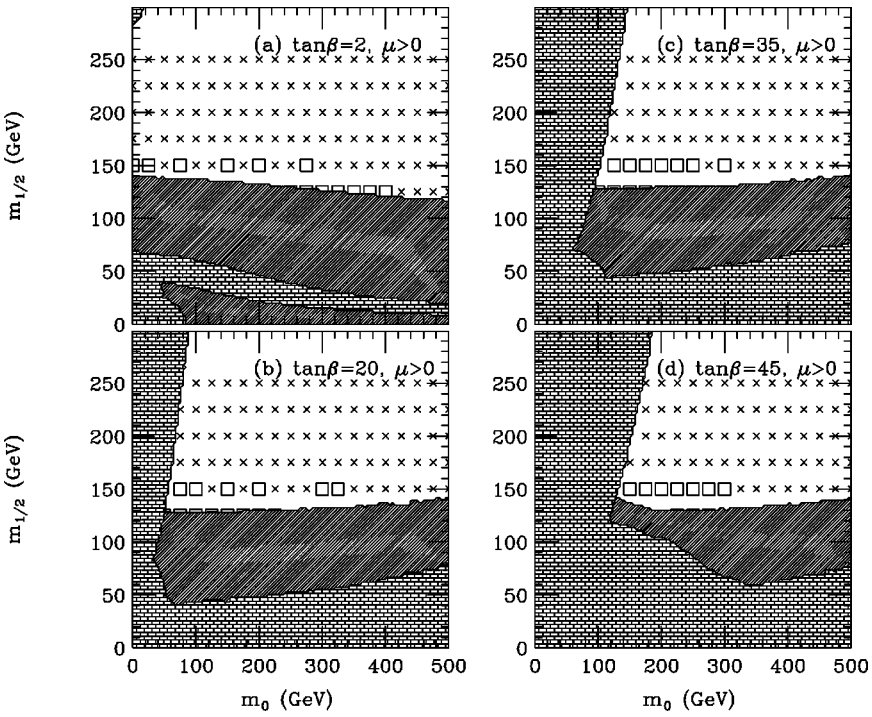

FIG. 5. Same as Fig. 4, except we require in addition that at least one of the jets be an identified *b* jet.

E_T^c value is more efficient in maximizing signal-to-background for large $m_{1/2}$ than requiring an extra *b* jet. However, for large m_0 and $m_{1/2} \sim 125-150$ GeV, the extra *b* tag does somewhat increase the reach of TeV33 for SUSY. Comparison of Figs. 4 and 5 shows three additional points accessible in frame (a), two in frame (b), and one in frame (d). We have also tried to extend the parameter space reach by requiring an identified τ jet (J0LT) or either a τ or *b* jet (J0LBT) along with $E_T^{\rm miss}$+jets. In both of these cases, no additional reach was achieved beyond the results of Figs. 4 and 5.

C. Reach via the JOS and JSS channels

The reach of Tevatron upgrades on the JOS channel is presented in Fig. 6. We require, in addition to the conditions at the beginning of this section events with exactly two opposite sign isolated leptons (e and μ), with $E_T(l_1) > 10$ GeV and a veto of τ jets. At the Tevatron at low tan β, signals in this channel mainly come from $\widetilde{W}_1\widetilde{Z}_2$ production, where $\widetilde{Z}_2$ decays leptonically, and $\widetilde{W}_1$ decays hadronically, while top production is a major source of SM background. There is significant reach by the Tevatron MI and TeV33 in this channel at low tan β, as seen in frame (a). As tan β increases, the $\widetilde{Z}_2$ leptonic branching fraction decreases (see Fig. 2), so that the MI has no reach in this channel for tan $\beta \geqslant 20$. The reach of TeV33 is severely limited in this channel at high tan β as well.

We have also examined the reach of the MI and TeV33 for same-sign dileptons (JSS channel), where we require in addition events to contain exactly two same sign isolated leptons, again with $E_T(l_1) > 10$ GeV and a veto of τ jets. The reach of Tevatron upgrades in this channel for MSUGRA is not very promising. The signal should result mainly from $\widetilde{g}\widetilde{g}$ and $\widetilde{g}\widetilde{q}$ production mechanisms, but these have only small cross sections for parameter space points beyond the reach of LEP2. We found almost no reach for MSUGRA in this channel beyond the LEP2 bounds for *any* values of tan β.

We have also studied the Tevatron reach in the dilepton plus jets channels where we required in addition that at least one of the leptons be a tagged τ jet: the JOST and JSST channels. In each of these cases, a small increase in reach was obtained for large values of tan β and low m_0 beyond the corresponding ''tauless'' channels. Most of this additional region can also be probed via the J3L channel discussed below, so we do not show these results here.

D. Reach via the J3L channel

For small values of tan β, the J3L channel considerably increases the region of MSUGRA parameters beyond what can be probed via the $E_T^{\rm miss}$ channel at a high luminosity Tevatron. In addition to the generic cuts for all the signals involving jets, we require the following analysis cuts for the J3L channel: events containing exactly three isolated leptons with $E_T(l_1) > 10$ GeV and a veto of τ jets plus we veto events with $|M(l^+l^-) - M_Z| < 8$ GeV. The reach in the J3L channel after all cuts are imposed is shown in Fig. 7. Since the signal almost always involves a leptonically decaying $\widetilde{Z}_2$, it is not surprising to see that the large reach at low tan β is gradually diminished until there is almost no reach for tan $\beta \sim 45$.

We have also examined the Tevatron reach in the trilepton plus jets channels where we required in addition that at least one of the leptons be a tagged τ jet: the J3LT channel.

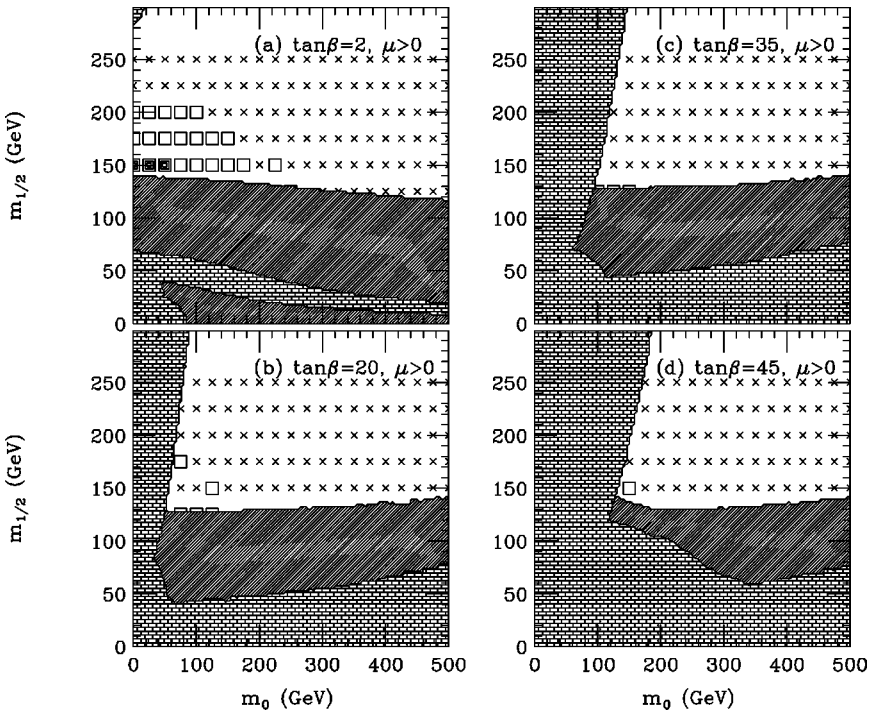

FIG. 6. A plot of the reach of the Tevatron MI and TeV33 for MSUGRA via the IOS signal.

As before, only a slight additional reach was obtained at large tan β and low m_0 beyond what could be probed via the ''tauless'' J3L channel. Here, and in the jetty dilepton channels mentioned above, this is presumably because secondary leptons from tau decay tend to be soft, and fail to satisfy the acceptance requirements. Again, we do not show these results here.

E. Reach via the C3L and C3LT channels

For small tan $\beta \sim 2$, and a large enough integrated luminosity, the maximum reach of the Tevatron was often achieved via the clean trilepton channel from $\tilde{W}_1\tilde{Z}_2 \to 3l + E_T^{\rm miss}$. For the C3L signal, following our earlier analysis [4] we implement the following cuts: we require three *iso-*

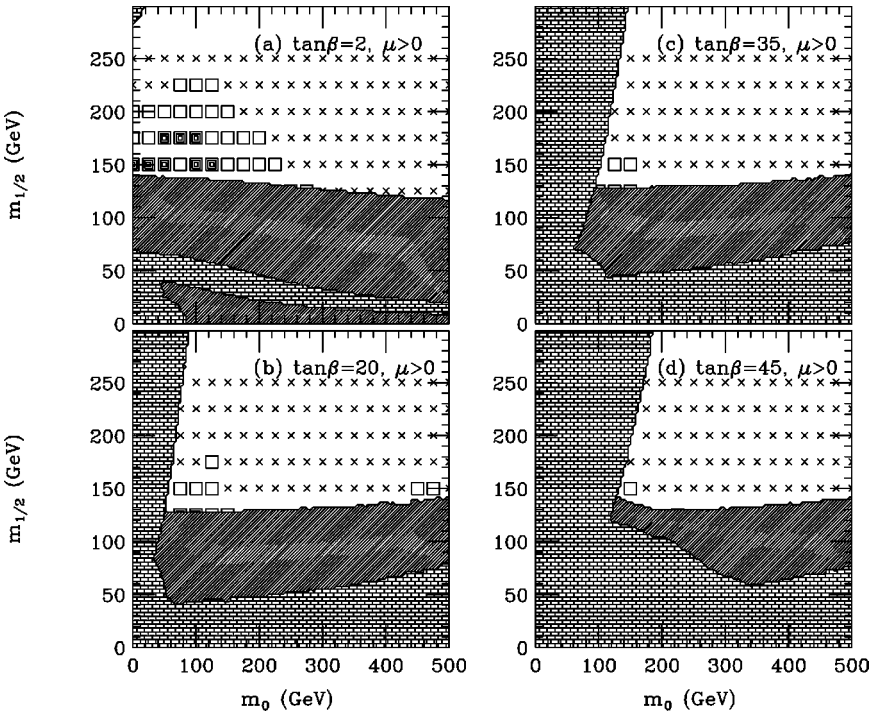

FIG. 7. A plot of the reach of the Tevatron MI and TeV33 for MSUGRA via the J3L signal.

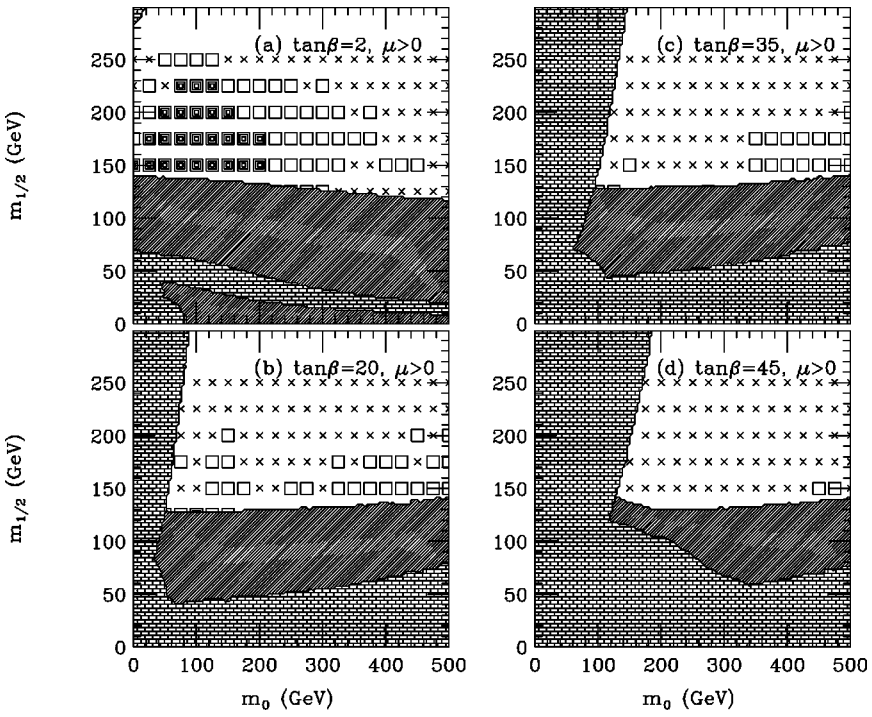

FIG. 8. A plot of the reach of the Tevatron MI and TeV33 for MSUGRA via the C3L signal.

lated leptons (e and μ) within $|\eta_l|<2.5$ in each event, with $E_T(l_1)>20$ GeV, $E_T(l_2)>15$ GeV, and $E_T(l_3)>10$ GeV; we require $E_T^{\rm miss}>25$ GeV; we require that the invariant mass of any opposite-sign, same flavor dilepton pair not reconstruct the Z mass, i.e., we require that $|m(ll)-M_Z| \geqslant 8$ GeV; we finally require the events to be *clean*, i.e., we veto events with jets. Our calculated background in this channel is 0.2 fb.

In Fig. 8, we show the reach in the C3L channel for the four cases of tan β. In frame (a), we see at low tan β that indeed there is no reach beyond the current LEP2 bound in the C3L channel for 0.1 fb^{-1}. For the MI integrated luminosity, however, there is considerable reach to values of $m_{1/2} \sim 225$ GeV, and for TeV33, the reach extends to $m_{1/2} \sim 250$ GeV, corresponding to $m_{\tilde{g}} \sim 700$ GeV. As tan β increases, the branching fraction for a leptonic decay of $\tilde{Z}_2$ and $\tilde{W}_1$ decrease. In frame (b), in fact, we find *no* reach for SUSY via the C3L channel for MI and considerably reduced reach for TeV33, except at large m_0. For smaller values of m_0 a complicated interference between various amplitudes reduces the leptonic decay width of $\tilde{Z}_2$. As tan β increases even further to 35 and 45 as in frames (c) and (d), the C3L reach is wiped out at low m_0. Some reach remains at large m_0 in frame (c), where the branching fraction BF($\tilde{Z}_2 \rightarrow ll\tilde{Z}_1$)$\sim$BF($Z \rightarrow ll$). In frame (d), most of this region also becomes inaccessible because of the increased importance of (virtual) Higgs boson mediated decays of $\tilde{Z}_2$ which lead to a strong enhancement of its decay to $bb\tilde{Z}_1$.

We have also examined the reach for clean trileptons, where one of the leptons is actually an identified τ jet (C3LT). In this case, we relax the additional p_T requirements on the leptons. This increases the chance of detecting the softer secondary leptons from the decay of tau(s). Trigger 4 presumably plays an important role for this class of events. The reach via this channel is shown in Fig. 9. In frames (b)–(d), significant additional reach is gained in the low m_0 regions, beyond that shown in any of the previous figures. Notice that the region where the signal is observable is where chargino and neutralino decays to real $\tilde{\tau}_1$ are accessible (see Fig. 3). The reach in the C3LT channel effectively extends the reach of TeV33 to $m_{1/2} \sim 250$ GeV for at least some value of m_0 for all the values of large tan β considered. We remark that the gain in reach via channels involving taus is limited because we require the presence of additional hard leptons (e or μ), jets or $E_T^{\rm miss}$ in order to be able to trigger on the event. Because secondary leptons from the decay of a tau tend to be soft, the development of an efficient τ trigger may significantly enhance the reach when tan β is large.

F. Reach via the COS and COST channels

In our previous studies [4] we had already noted that for small values of tan β, a study of the clean opposite sign dilepton channel (COS) would allow a confirmation of the signal in the C3L channel for a large range of MSUGRA parameters. For the COS channel, we require the following.

(i) Exactly two *isolated* OS's (either e or μ) leptons in each event, with $E_T(l_1)>10$ GeV and $E_T(l_2)>7$ GeV, and $|\eta(l)|<2.5$. In addition, we require *no* jets, which effectively reduces most of the tt background.

(ii) We require $E_T^{\rm miss}>25$ GeV to remove backgrounds from Drell-Yan dilepton production, and also the bulk of the background from $\gamma^*, Z \rightarrow \tau\tau$ decay.

(iii) We require $\phi(ll)<150°$, to further reduce $\gamma^*, Z \rightarrow \tau\tau$ background.

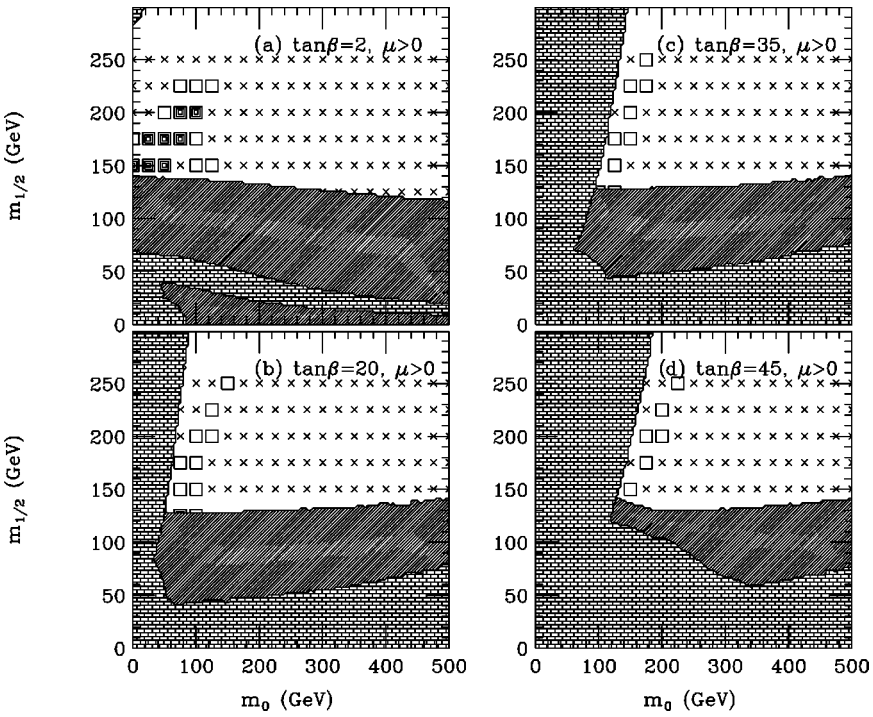

FIG. 9. A plot of the reach of the Tevatron MI and TeV33 for MSUGRA via the C3LT signal.

(iv) We require the Z mass cut: invariant mass of any opposite-sign, same flavor dilepton pair not reconstruct the Z mass, i.e., $|m(ll)-M_Z|>8$ GeV. Finally, we require $B=|\overrightarrow{E_T^{\rm miss}}|+|p_T(l_1)|+|p_T(l_2)|<100$ GeV. Our calculated background in this case is 64 fb.

We have checked that while there is an observable signal at the MI (TeV33) for $m_{1/2}\sim 150$ (175) GeV, and if $m_0 \lesssim 100$ GeV, there is no observable signal for any of the allowed regions of the plane if $\tan\beta \geqslant 20$. We have also examined this channel by requiring in addition that at least one of the leptons be an identified τ jet (COST). In this case, no reach for MSUGRA was found for any of the $\tan\beta$ values considered. We therefore do not show these figures.

G. Variation of signal with the *A* parameter

Up to now, we have fixed the parameter A_0 to be zero which, of course, does not mean that the A parameters vanish at the weak scale. To give the reader some idea of the variation of the $\widetilde{W}_1$ and $\widetilde{Z}_2$ branching fractions and of the important signals with A_0, we show in Fig. 10 the branching fractions for (a) $\widetilde{W}_1$ decay, (b) $\widetilde{Z}_2$ decay, and (c) sample signal cross sections for $m_0=m_{1/2}=150$ GeV and $\tan\beta=35$. The curves are terminated at A_0 values for which $\tilde{\tau}_1$ becomes the lightest sparticle. In frames (a) and (b) we see that the branching fraction three body decays to tau increases as the mass gap between the lighter stau and the chargino or neutralino reduces until the decays $\widetilde{W}_1\to\tilde{\tau}_1\nu$ and $\widetilde{Z}_2\to\tau\tilde{\tau}_1$ become allowed. This occurs at the extreme left and the extreme right of the plots, where the branching fraction for these decays (which are the only accessible two body decays) becomes essentially unity. The spikes near $A_0=-100$ GeV are an artifact: in ISAJET, the three-body decays are turned off when the neutralino mass equals the stau mass rather than $m_{\tilde{\tau}_1}+m_\tau$, where the two-body decay becomes accessible.

In frame (c) we show cross sections for the four event topologies which establish the total reach of the Tevatron as discussed in the last section. For the jetty channels, we use $E_T^c=60$ GeV. The cross section in the $E_T^{\rm miss}$ channel is rather insensitive to A_0 as might have been anticipated. The cross section in the J0LB channel appears to increase as A_0 varies from large positive values to the most negative values in the figure. This may seem surprising since neutralinos no longer decay into bottom jets. We have checked that for large negative values of A_0 the t squark becomes relatively light, and since it decays via $\tilde{t}_1\to b\widetilde{W}_1$, it is a significant source of such events. Another surprising feature of the figure is that the C3LT cross sections do not show a large increase at the edges of the curve where decays to taus dominate. The reason is that at the extreme ends, $|m_{\tilde{\tau}_1}-m_{\tilde{Z}_1}|$ becomes small, so that the daughter tau in $\tilde{\tau}_1\to\widetilde{Z}_1\tau$ becomes soft and fails to pass our acceptance cuts. Indeed this mass difference is just 4 GeV for the case $A_0=-300$ GeV, which explains why this cross section actually *decreases*. We see that the C3L cross section is surprisingly constant over the entire range of A_0, even for the cases of large positive A_0. For $A_0=500$ GeV, we have checked that $\widetilde{W}_1\widetilde{Z}_2$ is indeed a subdominant source of C3L events. In this case, most trileptons come from slepton production (mainly $\tilde{l}\tilde{\nu}$), but there is a substantial contribution from the production of the heavier charginos and neutralinos; $\widetilde{W}_2$ decays into real W as well as into sleptons, while $\widetilde{Z}_3$ can decay to real W or Z as well as to sleptons. There is thus a plethora of sources for these events. We expect that this is true for other A_0 values also. Finally, we

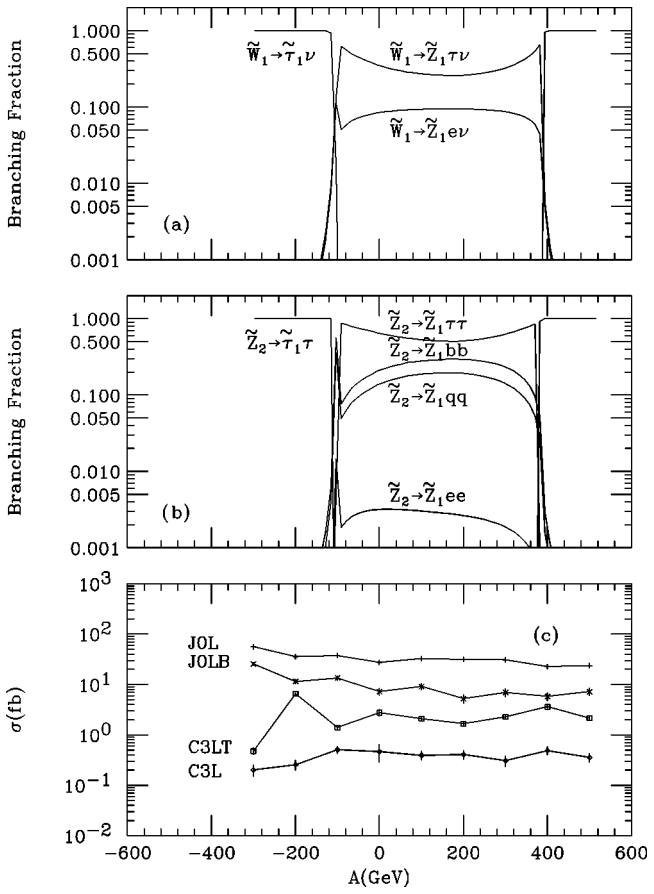

FIG. 10. The dependence of (a) $\widetilde{W}_1$ branching fractions, (b) $\widetilde{Z}_2$ branching fractions, and (c) cross sections for selected topologies on the model parameter A_0. We fix $m_0 = m_{1/2} = 150$ GeV and choose $\tan\beta = 35$ for illustration. In frame (c) we also show the error bars in our calculation of the cross sections which are due to Monte Carlo integration.

remark that the signal cross sections vary much less with A_0 than might have been anticipated from the variations in the branching fractions. We caution the reader that we have not made an exhaustive investigation of whether or not this statement remains true for all values of m_0, $m_{1/2}$, and $\tan\beta$.

IV. SUMMARY AND CONCLUSIONS

To summarize the reach of Tevatron upgrades for large and small $\tan\beta$, we show in Fig. 11 the SUSY reach via all of the channels that were examined, for both the upgrade options of the Tevatron. Thus, if a parameter space point is accessible via any channel, we place an appropriate box, corresponding to the integrated luminosity that is required. The cumulative reach shown in the figure is completely established with just four channels: J0L, J0LB, C3L, and C3LT. For some points, the signal may be observable in more than one of these or other channels studied in this paper. It is possible that some additional reach may be gained by combining several channels to gain a net ''5σ'' signal, even though the significance in each of these channels is somewhat smaller. We do not consider this added detail here.

We see from Fig. 11 that as $\tan\beta$ increases, the SUSY reach of Tevatron upgrades is significantly reduced. For the MI option, there is no reach beyond current LEP2 bounds that can be established at $\tan\beta = 45$. The TeV33 option has some reach in all frames, but clearly a much reduced reach for large $\tan\beta$. In particular, there are parameter regions just beyond the current LEP2 bounds for which there will be *no observable signal* even with the luminosity of TeV33. The reduction of the reach is mostly due to the depletion of leptonic signals, especially the clean three lepton signal, in the region of large $\tan\beta$. Note that the branching ratio for $\widetilde{W}_1$ and $\widetilde{Z}_2$ to decay into electrons and muons plus missing particles is actually quite large if charginos and neutralinos dominantly decay into real or virtual $\widetilde{\tau}_1$. However, the secondary leptons produced in subsequent τ decays are usually too soft to pass our trigger criteria or acceptance cuts. It might be worthwhile to investigate whether these cuts can be lowered without introducing unacceptably large backgrounds (e.g., from heavy flavors, where the lepton happens to be isolated and the jet is lost, or from jets faking leptons) or via a development of a special trilepton trigger.

Modes with identified (hadronically decaying) taus could only partly compensate this loss of reach in the leptonic channels. Again the problem seems to be that the hadronic decay products of the τ leptons are frequently too soft to pass the cut $E_T(\tau - \text{jet}) > 15$ GeV. It might be worthwhile to study if this cut can be lowered, e.g., by focusing only on one-prong τ decays, for which QCD backgrounds are much smaller than in the three-prong channel. In addition, the triggers adopted in our study are not very efficient for events with rather soft leptons plus τ jets, as in our C3LT sample. We therefore believe that the reach of future Tevatron runs could be extended significantly in the region of large $\tan\beta$ if it is possible to devise strategies to reliably identify, and perhaps even trigger on taus with visible p_T smaller than 15 GeV. We remark, however, that even without such developments, experiments at the LHC will probe the entire parameter plane shown at least via the E_T^{miss} channel.

ACKNOWLEDGMENTS

We thank Vernon Barger for reading the manuscript. One of us (X.T.) is grateful for the hospitality of the Asia-Pacific Centre for Theoretical Physics where part of this work was carried out. H.B. and X.T. thank the Aspen Center for Physics for hospitality during the period that part of this work was done. This research was supported in part by the U.S. Department of Energy under Contract Nos. DE-FG05-87ER40319, DE-AC02-76CH00016, and DE-FG-03-94ER40833.

APPENDIX: SPARTICLE DECAY WIDTHS FOR LARGE $\tan\beta$

In this appendix we give analytical expressions for those three-body partial widths that are sensitive to b or τ Yukawa couplings and/or to $\widetilde{f}_L$-$\widetilde{f}_R$ mixing ($f = b, \tau$). We first list the relevant couplings, and then give results for $\widetilde{Z}_i \to \widetilde{Z}_j f\bar{f}$, $\widetilde{W}_i \to \tau\nu_\tau \widetilde{Z}_j$, $\widetilde{Z}_i \to \widetilde{W}_j f\bar{f}$, and $\widetilde{g} \to bt\widetilde{W}_i$.

Many of the couplings and kinematic functions that enter

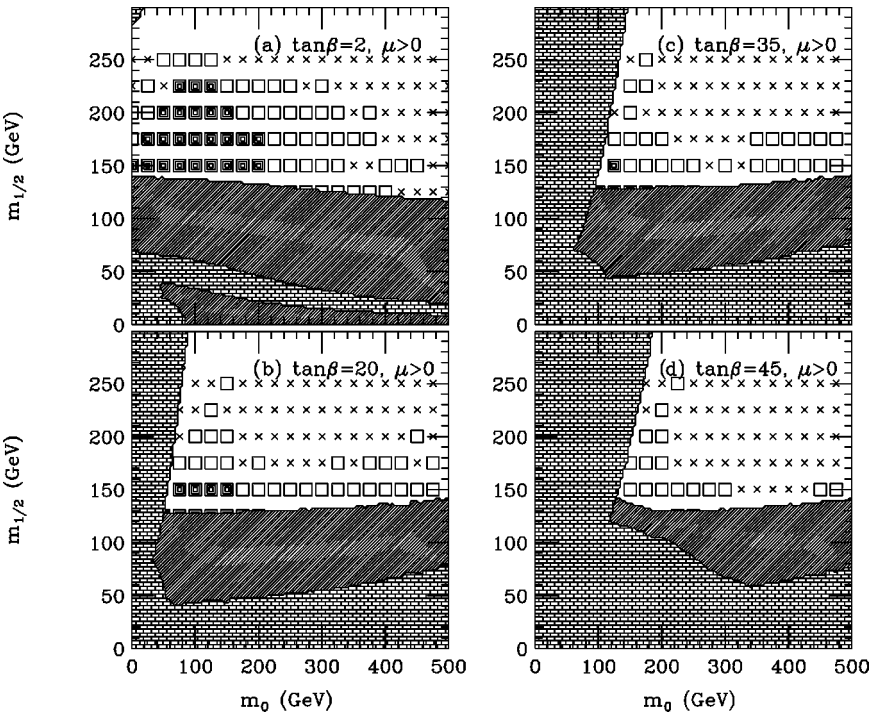

FIG. 11. A plot of the combined reach of the Tevatron MI and TeV33 for MSUGRA via *all* of the signal channels considered in this paper.

our computations have been defined in our earlier papers. Instead of rewriting these lengthy definitions again, we provide the reader with references to the papers from which these couplings are used. In these studies, the two charginos were denoted by $\tilde{W}_-$ and $\tilde{W}_+$ instead of $\tilde{W}_1$ and $\tilde{W}_2$, respectively. Also, the lighter (heavier) neutral *CP* even Higgs scalar was denoted by H_l (H_h) rather than by h (H), while the *CP* odd pseudoscalar was denoted by H_p rather than A. The corresponding couplings are characterized by superscripts *l*, *h*, and *p*. To facilitate the use of these couplings from the earlier literature, we use this older notation to denote the charginos and neutral Higgs bosons in the formulas listed in this Appendix.

1. Couplings

The couplings of electroweak neutralinos and charginos to a fermion and a sfermion are affected by mixing between SU(2) doublet (L-type) and singlet (R-type) sfermions. We write the sfermion mass eigenstates as

$$\tilde{f}_1 = \cos\,\theta_f \tilde{f}_L - \sin\,\theta_f \tilde{f}_R,$$

$$\tilde{f}_2 = \sin\,\theta_f \tilde{f}_L + \cos\,\theta_f \tilde{f}_R, \tag{A1}$$

where $\tilde{f}_1$ denotes the lighter eigenstate. Since there is no L-R mixing in the sneutrino sector, some couplings remain unaffected. We list these for completeness, using the notation of Refs. [18] and [19]:

$$\tilde{A}^{\nu}_{\tilde{Z}_i} = (g v_3^{(i)} - g' v_4^{(i)})/\sqrt{2}, \tag{A2a}$$

$$\tilde{A}^{\tau}_{\tilde{W}_-} = -g\,\sin\,\gamma_R, \tag{A2b}$$

$$\tilde{A}^{\nu}_{\tilde{W}_-} = -g\,\sin\,\gamma_L, \tag{A2c}$$

$$B^{\tau}_{\tilde{W}_-} = -f_\tau \cos\,\gamma_L. \tag{A2d}$$

Here, g and g' are the SU(2) and $\mathrm{U}(1)_Y$ gauge couplings, and f_f the Yukawa couplings of fermion f. The corresponding couplings of the heavier chargino mass eigenstate $\tilde{W}_+$ can be obtained by the substitutions [18]

$$\tilde{W}_- \to \tilde{W}_+ : \quad \cos\,\gamma_{L,R} \to -\theta_{x,y}\,\sin\,\gamma_{L,R},$$
$$\sin\,\gamma_{L,R} \to \theta_{x,y}\,\cos\,\gamma_{L,R}. \tag{A3}$$

In the calculation of the partial widths, we will ignore terms $\propto m_b, m_\tau$ when doing the Dirac traces. It then becomes convenient to write the matrix elements in terms of couplings to fermions with fixed chirality. In the following we denote all left-handed couplings with the symbol α, and right-handed couplings with β. The chargino couplings to the lighter third generation squark mass eigenstates can be written as

$$\alpha^{\tilde{t}_1}_{\tilde{W}_-} = -g\,\sin\,\gamma_R\,\cos\,\theta_t + f_t\,\cos\,\gamma_R\,\sin\,\theta_t, \tag{A4a}$$

$$\beta^{\tilde{t}_1}_{\tilde{W}_-} = -f_b\,\cos\,\gamma_L\,\cos\,\theta_t, \tag{A4b}$$

$$\alpha^{\tilde{b}_1}_{\tilde{W}_-} = -g \sin\gamma_L \cos\theta_b + f_b \cos\gamma_L \sin\theta_b, \tag{A4c}$$

$$\beta^{\tilde{b}_1}_{\tilde{W}_-} = -f_t \cos\gamma_R \cos\theta_b. \tag{A4d}$$

The corresponding couplings to third generation sleptons can be obtained by the substitutions

$$\tilde{q}\to\tilde{l}: \quad \theta_l\to 0, \quad \theta_b\to\theta_\tau, \quad f_t\to 0, \quad f_b\to f_\tau. \tag{A5}$$

Similarly, the couplings to the heavier sfermion mass eigenstates $\tilde{f}_2$ can be obtained by substituting:

$$\tilde{f}_1\to\tilde{f}_2: \quad \cos\theta_f\to\sin\theta_f, \quad \sin\theta_f\to-\cos\theta_f. \tag{A6}$$

Finally, the couplings of the heavier chargino state can again be computed using Eq. (A3).

The couplings of neutralinos to b and τ (s)fermions can be written as

$$\alpha^{\tilde{f}_1}_{\tilde{Z}_i} = \tilde{A}^f_{\tilde{Z}_i} \cos\theta_f - f_f v_2^{(i)} \sin\theta_f, \tag{A7a}$$

$$\beta^{\tilde{f}_1}_{\tilde{Z}_i} = f_f v_2^{(i)} \cos\theta_f + \tilde{B}^f_{\tilde{Z}_i} \sin\theta_f, \tag{A7b}$$

where $\tilde{A}^f_{\tilde{Z}_i}$, $\tilde{B}^f_{\tilde{Z}_i}$ are as in Ref. [19]. The couplings to fermions with weak isospin $I_3 = +1/2$ can be computed from Eqs. (A7) by inserting the corresponding unmixed couplings; in addition, one has to replace the component $v_2^{(i)}$ of the neutralino eigenvector by $v_1^{(i)}$. The couplings to heavier sfermion eigenstates can again be obtained by applying Eq. (A6).

Finally, we introduce the charged Higgs-boson–chargino–neutralino couplings

$$\alpha^{(i)}_{\tilde{W}_-} = \cos\beta A_2^{(i)}, \quad \beta^{(i)}_{\tilde{W}_-} = -\sin\beta A_4^{(i)}, \tag{A8a}$$

$$\alpha^{(i)}_{\tilde{W}_+} = \cos\beta A_1^{(i)}\theta_y, \quad \beta^{(i)}_{\tilde{W}_+} = -\sin\beta A_3^{(i)}\theta_x, \tag{A8b}$$

where i is the neutralino index; the $A_k^{(i)}$ can be found in Ref. [20].

2. $\tilde{Z}_j\to\tilde{Z}_i f\bar{f}$ decays

We are now in a position to present our results for the partial widths for decays involving third generation fermions. We begin with the decay of a neutralino into a lighter neutralino and a $b\bar{b}$ or $\tau^+\tau^-$ pair. This decay can proceed through the exchange of the two sfermion mass eigenstates $\tilde{f}_{1,2}$, through the exchange of a Z boson, or through the exchange of one of the three neutral Higgs bosons of the MSSM. The partial width can therefore be written as

$$\Gamma(\tilde{Z}_j\to\tilde{Z}_i f\bar{f}) = \frac{1}{2} N_c(f) \frac{1}{(2\pi)^5} \frac{1}{2m_{\tilde{Z}_j}} (\Gamma_{\tilde{f}} + \Gamma_Z + \Gamma_{H_{l,h}} + \Gamma_{H_p} + \Gamma_{Z\tilde{f}} + \Gamma_{H_{l,h}\tilde{f}} + \Gamma_{H_p\tilde{f}}), \tag{A9}$$

where the color factor $N_c(f) = 3\,(1)$ for $f = b\,(\tau)$. Recall that we set $m_f = 0$ when evaluating Dirac traces. As a result, the Higgs boson and Z exchange diagrams do not interfere with each other.[1]

The *pure sfermion exchange contribution* is given by

$$\Gamma_{\tilde{f}} = \Gamma_{\tilde{f}_1} + \Gamma_{\tilde{f}_2} + \Gamma_{\tilde{f}_{1,2}}, \tag{A10}$$

where

$$\Gamma_{\tilde{f}_k} = \Gamma^{\tilde{f}_k}_{LL} + \Gamma^{\tilde{f}_k}_{RR} + \Gamma^{\tilde{f}_k}_{LR} \quad (k=1,2), \tag{A11a}$$

$$\Gamma_{\tilde{f}_{1,2}} = \Gamma^{\tilde{f}_1}_L \Gamma^{\tilde{f}_2}_L + \Gamma^{\tilde{f}_1}_L \Gamma^{\tilde{f}_2}_R + \Gamma^{\tilde{f}_1}_R \Gamma^{\tilde{f}_2}_L + \Gamma^{\tilde{f}_1}_R \Gamma^{\tilde{f}_2}_R. \tag{A11b}$$

Here, the subscripts L and R refer to the chirality of the SM fermion coupling to the heavier neutralino $\tilde{Z}_j$. The quantities appearing in Eq. (A11) are

$$\Gamma^{\tilde{f}_k}_{LL} = 4(\alpha^{\tilde{f}_k}_{\tilde{Z}_j})^2 \{[(\alpha^{\tilde{f}_k}_{\tilde{Z}_i})^2 + (\beta^{\tilde{f}_k}_{\tilde{Z}_i})^2]\psi(m_{\tilde{Z}_j}, m_{\tilde{f}_k}, m_{\tilde{Z}_i}) + (-1)^{\theta_i+\theta_j}(\alpha^{\tilde{f}_k}_{\tilde{Z}_i})^2 \phi(m_{\tilde{Z}_j}, m_{\tilde{f}_k}, m_{\tilde{Z}_i})\}, \tag{A12a}$$

$$\Gamma^{\tilde{f}_k}_{RR} = 4(\beta^{\tilde{f}_k}_{\tilde{Z}_j})^2 \{[(\alpha^{\tilde{f}_k}_{\tilde{Z}_i})^2 + (\beta^{\tilde{f}_k}_{\tilde{Z}_i})^2]\psi(m_{\tilde{Z}_j}, m_{\tilde{f}_k}, m_{\tilde{Z}_i}) + (-1)^{\theta_i+\theta_j}(\beta^{\tilde{f}_k}_{\tilde{Z}_i})^2 \phi(m_{\tilde{Z}_j}, m_{\tilde{f}_k}, m_{\tilde{Z}_i})\}, \tag{A12b}$$

$$\Gamma^{\tilde{f}_k}_{LR} = -8\alpha^{\tilde{f}_k}_{\tilde{Z}_j}\beta^{\tilde{f}_k}_{\tilde{Z}_j}\alpha^{\tilde{f}_k}_{\tilde{Z}_i}\beta^{\tilde{f}_k}_{\tilde{Z}_i} Y(m_{\tilde{Z}_j}, m_{\tilde{f}_k}, m_{\tilde{f}_k}, m_{\tilde{Z}_i}), \tag{A12c}$$

[1]This would be a very bad approximation for $\tilde{Z}_j\to\tilde{Z}_i t\bar{t}$ decays. However, if these decays are allowed, $\tilde{Z}_j$ has numerous two-body decay modes into real gauge and Higgs bosons and lighter neutralinos and charginos. The branching ratios for neutralino three-body decays into top quarks are therefore always negligibly small. Analogous remarks apply to $\tilde{W}_j\to\tilde{Z}_i t\bar{b}$ decays.

$$\Gamma_L^{\tilde{f}_1}\Gamma_L^{\tilde{f}_2}=8\alpha_{\tilde{Z}_j}^{\tilde{f}_1}\alpha_{\tilde{Z}_j}^{\tilde{f}_2}\{[\alpha_{\tilde{Z}_i}^{\tilde{f}_1}\alpha_{\tilde{Z}_i}^{\tilde{f}_2}+\beta_{\tilde{Z}_i}^{\tilde{f}_1}\beta_{\tilde{Z}_i}^{\tilde{f}_2}]\tilde{\psi}(m_{\tilde{Z}_j},m_{\tilde{f}_1},m_{\tilde{f}_2},m_{\tilde{Z}_i})+(-1)^{\theta_i+\theta_j}\alpha_{\tilde{Z}_i}^{\tilde{f}_1}\alpha_{\tilde{Z}_i}^{\tilde{f}_2}\tilde{\phi}(m_{\tilde{Z}_j},m_{\tilde{f}_1},m_{\tilde{f}_2},m_{\tilde{Z}_i})\}, \tag{A12d}$$

$$\Gamma_R^{\tilde{f}_1}\Gamma_R^{\tilde{f}_2}=8\beta_{\tilde{Z}_j}^{\tilde{f}_1}\beta_{\tilde{Z}_j}^{\tilde{f}_2}\{[\alpha_{\tilde{Z}_i}^{\tilde{f}_1}\alpha_{\tilde{Z}_i}^{\tilde{f}_2}+\beta_{\tilde{Z}_i}^{\tilde{f}_1}\beta_{\tilde{Z}_i}^{\tilde{f}_2}]\tilde{\psi}(m_{\tilde{Z}_j},m_{\tilde{f}_1},m_{\tilde{f}_2},m_{\tilde{Z}_i})+(-1)^{\theta_i+\theta_j}\beta_{\tilde{Z}_i}^{\tilde{f}_1}\beta_{\tilde{Z}_i}^{\tilde{f}_2}\tilde{\phi}(m_{\tilde{Z}_j},m_{\tilde{f}_1},m_{\tilde{f}_2},m_{\tilde{Z}_i})\}, \tag{A12e}$$

$$\Gamma_L^{\tilde{f}_1}\Gamma_R^{\tilde{f}_2}=-8\alpha_{\tilde{Z}_j}^{\tilde{f}_1}\beta_{\tilde{Z}_j}^{\tilde{f}_2}\alpha_{\tilde{Z}_i}^{\tilde{f}_2}\beta_{\tilde{Z}_i}^{\tilde{f}_1}Y(m_{\tilde{Z}_j},m_{\tilde{f}_1},m_{\tilde{f}_2},m_{\tilde{Z}_i}), \tag{A12f}$$

$$\Gamma_L^{\tilde{f}_2}\Gamma_R^{\tilde{f}_1}=-8\alpha_{\tilde{Z}_j}^{\tilde{f}_2}\beta_{\tilde{Z}_j}^{\tilde{f}_1}\alpha_{\tilde{Z}_i}^{\tilde{f}_1}\beta_{\tilde{Z}_i}^{\tilde{f}_2}Y(m_{\tilde{Z}_j},m_{\tilde{f}_1},m_{\tilde{f}_2},m_{\tilde{Z}_i}). \tag{A12g}$$

The kinematic functions ψ, ϕ, and Y are given in Ref. [21],[2] and θ_i is 0 (1) if the sign of the ith eigenvalue of the neutralino mass matrix is positive (negative) [18]. The functions $\tilde{\psi}$ and $\tilde{\phi}$, which depend on two sfermion masses are generalizations of the functions ψ and ϕ which depend on just one sfermion mass: to define $\tilde{\psi}$, we simply split the squared factor where the top squark mass occurs in Eq. (A6a) of Ref. [21], into two such factors, with each one containing a different sfermion mass. Similarly, $\tilde{\phi}$ is generalized from ϕ by writing $m_{\tilde{f}_1}$ in the first factor outside the square parenthesis in Eq. (A6b) of Ref. [21], and $m_{\tilde{f}_2}$ inside the square parenthesis. In other words, when the two sfermions $\tilde{f}_1$ and $\tilde{f}_2$ have the same mass, $\tilde{\psi}=\psi$ and $\tilde{\phi}=\phi$.

For completeness, we also give the *squared Z exchange contribution*, which is not affected by sfermion mixing:

$$\begin{aligned}\Gamma_Z=&128e^2|W_{ij}|^2(\alpha_f^2+\beta_f^2)m_{\tilde{Z}_j}\frac{\pi^2}{2}\\&\times\int_{m_{\tilde{Z}_i}}^{E_{\max}}dE\,\frac{B_f\sqrt{E^2-m_{\tilde{Z}_i}^2}}{(m_{\tilde{Z}_i}^2+m_{\tilde{Z}_j}^2-M_Z^2-2Em_{\tilde{Z}_j})^2}\\&\times\Bigg\{E[m_{\tilde{Z}_i}^2+m_{\tilde{Z}_j}^2-(-1)^{\theta_i+\theta_j}2m_{\tilde{Z}_i}m_{\tilde{Z}_j}]\\&-m_{\tilde{Z}_j}\left(E^2+m_{\tilde{Z}_i}^2+\frac{B_f}{3}(E^2-m_{\tilde{Z}_i}^2)\right)\\&+(-1)^{\theta_i+\theta_j}m_{\tilde{Z}_i}(m_{\tilde{Z}_i}^2+m_{\tilde{Z}_j}^2-2m_f^2)\Bigg\}.\end{aligned} \tag{A13}$$

Here, e is the QED coupling, W_{ij} is the $Z\tilde{Z}_i\tilde{Z}_j$ coupling given in Ref. [22], and α_f, β_f are the left- and right-handed Zff couplings in the notation of Ref. [23]. Finally, the upper integration limit is given by

$$E_{\max}=\frac{m_{\tilde{Z}_i}^2+m_{\tilde{Z}_j}^2-4m_f^2}{2m_{\tilde{Z}_j}} \tag{A14}$$

and

$$B_f=\sqrt{1-\frac{4m_f^2}{m_{\tilde{Z}_i}^2+m_{\tilde{Z}_j}^2-2Em_{\tilde{Z}_j}}}. \tag{A15}$$

The *pure scalar Higgs boson exchange contribution* can also be written as a single integral:

$$\begin{aligned}\Gamma_{H_{l,h}}=&2\pi^2\left(\frac{gm_f}{M_W\cos\beta}\right)^2m_{\tilde{Z}_j}\int_{m_{\tilde{Z}_i}}^{E_{\max}}dEB_f\sqrt{E^2-m_{\tilde{Z}_i}^2}\\&\times(m_{\tilde{Z}_i}^2+m_{\tilde{Z}_j}^2-2m_{\tilde{Z}_j}E-2m_f^2)[E+(-1)^{\theta_i+\theta_j}m_{\tilde{Z}_i}]\\&\times\left[\frac{\sin\alpha(X_{ij}^l+X_{ji}^l)}{m_{\tilde{Z}_i}^2+m_{\tilde{Z}_j}^2-2m_{\tilde{Z}_j}E-m_{H_l}^2}\right.\\&\left.+\frac{\cos\alpha(X_{ij}^h+X_{ji}^h)}{m_{\tilde{Z}_i}^2+m_{\tilde{Z}_j}^2-2m_{\tilde{Z}_j}E-m_{H_h}^2}\right]^2.\end{aligned} \tag{A16}$$

Here, $X_{ij}^{l,h}$ are the couplings of the light and heavy neutral scalar Higgs boson to two neutralinos and α is the angle describing mixing in the scalar Higgs sector as defined in Ref. [20], and $m_{H_{lh}}^2$ are the masses of the two Higgs bosons. The upper integration limit is again given by Eq. (A14).

The *squared pseudoscalar Higgs boson exchange contribution* can be cast in a quite similar form:

[2]Note that the third line in Eq. (A6h) of that paper should come with a positive overall sign. Furthermore, the last term in the first denominator in Eq. (A6a) should be m_t^2, rather than m_t^2. Of course, m_t is repaced by the appropriate fermion mass in the definition of these functions. Finally, although the number of arguments appearing in the Y function are different from that in Ref. [21], the correspondence is obvious.

$$\Gamma_{H_p}=2\pi^2\left[\frac{gm_f\tan\beta}{M_W}(X^p_{ij}+X^p_{ji})\right]^2 m_{\tilde{Z}_j}\times\int_{m_{\tilde{Z}_i}}^{E_{\max}}dE B_f\sqrt{E^2-m^2_{\tilde{Z}_i}}\times\frac{(m^2_{\tilde{Z}_i}+m^2_{\tilde{Z}_j}-2m_{\tilde{Z}_j}E-2m_f^2)[E-(-1)^{\theta_i+\theta_j}m_{\tilde{Z}_i}]}{(m^2_{\tilde{Z}_i}+m^2_{\tilde{Z}_j}-2m_{\tilde{Z}_j}E-m^2_{H_p})^2}. \tag{A17}$$

The couplings X^p_{ij} can again be found in Ref. [20].

We now turn to the various interference terms listed in Eq. (A9). The *Z-sfermion interference contributions* can be written as

$$\Gamma_{Z\tilde{f}}=\Gamma_{Z\tilde{f}_1}+\Gamma_{Z\tilde{f}_2}, \tag{A18}$$

with

$$\Gamma_{Z\tilde{f}_k}=32e\tilde{W}_{ij}[\alpha^{\tilde{f}_k}_{\tilde{Z}_i}\alpha^{\tilde{f}_k}_{\tilde{Z}_j}(\alpha_f-\beta_f)-\beta^{\tilde{f}_k}_{\tilde{Z}_i}\beta^{\tilde{f}_k}_{\tilde{Z}_j}(\alpha_f+\beta_f)]\frac{\pi^2}{2m_{\tilde{Z}_j}}\times\int_{4m_f^2}^{(m_{\tilde{Z}_j}-m_{\tilde{Z}_i})^2}\frac{ds}{s-M_Z^2}\times\Bigg\{-\frac{1}{2}Q'(m_{\tilde{Z}_j}E_Q+m^2_{\tilde{f}_k}-m^2_{\tilde{Z}_j}-s-m_f^2)-\frac{1}{4m_{\tilde{Z}_j}}[(m^2_{\tilde{f}_k}-m^2_{\tilde{Z}_i}-m_f^2)(m^2_{\tilde{f}_k}-m^2_{\tilde{Z}_j}-m_f^2)+(-1)^{\theta_i+\theta_j}m_{\tilde{Z}_i}m_{\tilde{Z}_j}(s-2m_f^2)]\times\log\frac{m_{\tilde{Z}_j}(E_Q+Q')-\mu^2}{m_{\tilde{Z}_j}(E_Q-Q')-\mu^2}\Bigg\}. \tag{A19}$$

Here we have introduced the quantities

$$\mu^2=s+m^2_{\tilde{f}_k}-m^2_{\tilde{Z}_i}-m_f^2,\quad E_Q=\frac{s+m^2_{\tilde{Z}_j}-m^2_{\tilde{Z}_i}}{2m_{\tilde{Z}_j}},$$

$$Q=\sqrt{E_Q^2-s}, \tag{A20}$$

and

$$Q'=Q\sqrt{1-\frac{4m_f^2}{s}}.$$

The real coupling $\tilde{W}_{mn}$ is defined to be

$$\tilde{W}_{mn}=(-i)^{\theta_m+\theta_n}(-1)^{\theta_m}W_{mn}, \tag{A21}$$

with W_{mn} given in Ref. [22].

Finally, the *Higgs-sfermion interference contributions* can be written as

$$\Gamma_{H_{l,h,p}\tilde{f}}=\Gamma_{H_{l,h,p}\tilde{f}_1}+\Gamma_{H_{l,h,p}\tilde{f}_2}, \tag{A22}$$

where H_l, H_h, and H_p again denote the light scalar, heavy scalar, and pseudoscalar Higgs boson, respectively. The separate contributions in Eq. (A22) are given by

$$\Gamma_{H_l\tilde{f}_k}=\frac{2\pi^2}{m_{\tilde{Z}_j}}\frac{gm_f\sin\alpha}{M_W\cos\beta}(X^l_{ji}+X^l_{ij})[\alpha^{\tilde{f}_k}_{\tilde{Z}_i}\beta^{\tilde{f}_k}_{\tilde{Z}_j}+\alpha^{\tilde{f}_k}_{\tilde{Z}_j}\beta^{\tilde{f}_k}_{\tilde{Z}_i}]\times(-1)^{\theta_i+\theta_j}J_H(m_{\tilde{Z}_j},m_{\tilde{f}_k},m_{H_l},m_{\tilde{Z}_i},\theta_i+\theta_j), \tag{A23a}$$

$$\Gamma_{H_h\tilde{f}_k}=\frac{2\pi^2}{m_{\tilde{Z}_j}}\frac{gm_f\cos\alpha}{M_W\cos\beta}(X^h_{ji}+X^h_{ij})[\alpha^{\tilde{f}_k}_{\tilde{Z}_i}\beta^{\tilde{f}_k}_{\tilde{Z}_j}+\alpha^{\tilde{f}_k}_{\tilde{Z}_j}\beta^{\tilde{f}_k}_{\tilde{Z}_i}]\times(-1)^{\theta_i+\theta_j}J_H(m_{\tilde{Z}_j},m_{\tilde{f}_k},m_{H_h},m_{\tilde{Z}_i},\theta_i+\theta_j), \tag{A23b}$$

$$\Gamma_{H_p\tilde{f}_k}=\frac{2\pi^2}{m_{\tilde{Z}_j}}\frac{gm_f\tan\beta}{M_W}(X^p_{ji}+X^p_{ij})[\alpha^{\tilde{f}_k}_{\tilde{Z}_i}\beta^{\tilde{f}_k}_{\tilde{Z}_j}+\alpha^{\tilde{f}_k}_{\tilde{Z}_j}\beta^{\tilde{f}_k}_{\tilde{Z}_i}]\times(-1)^{1+\theta_i+\theta_j}J_H(m_{\tilde{Z}_j},m_{\tilde{f}_k},m_{H_p},m_{\tilde{Z}_i},1+\theta_i+\theta_j). \tag{A23c}$$

The function J_H is defined as

$$J_H(m_{\tilde{Z}_j},m_{\tilde{f}},m_H,m_{\tilde{Z}_i},\theta)=\int_{4m_f^2}^{(m_{\tilde{Z}_j}-m_{\tilde{Z}_i})^2}\frac{ds}{s-m_H^2}\Bigg[\frac{1}{2}sQ'+\frac{sm_f^2-m_f^2(m^2_{\tilde{Z}_i}+m^2_{\tilde{Z}_j})+(-1)^\theta m_{\tilde{Z}_i}m_{\tilde{Z}_j}(s-2m_f^2)}{4m_{\tilde{Z}_j}}\times\log\frac{m_{\tilde{Z}_j}(E_Q+Q')-\mu^2}{m_{\tilde{Z}_j}(E_Q-Q')-\mu^2}\Bigg], \tag{A24}$$

where μ^2, E_Q, Q, and Q' have been defined in Eq. (A20).

3. $\tilde{W}_j\to\tilde{Z}_i\tau\nu_\tau$ decays

These decays proceed via the exchange of a W boson, a charged or neutral third generation slepton, or a charged Higgs boson. The partial widths can thus be written as

$$\Gamma(\tilde{W}_j^-\to\tilde{Z}_i\tau^-\overline{\nu}_\tau)=\frac{1}{2}\frac{1}{(2\pi)^5}\frac{1}{2m_{\tilde{W}_j}}(\Gamma_W+\Gamma_{\tilde{\nu}}+\Gamma_{\tilde{\tau}}+\Gamma_H+\Gamma_{W\tilde{\nu}}+\Gamma_{W\tilde{\tau}}+\Gamma_{\tilde{\nu}\tilde{\tau}}+\Gamma_{H\tilde{\nu}}+\Gamma_{H\tilde{\tau}}). \tag{A25}$$

The Higgs and W exchange contributions do not interfere, since we neglected terms $\propto m_\tau$ when doing the Dirac algebra.

The *squared W exchange contribution* is given by

$$\Gamma_W = 4g^4 \frac{\pi^2}{3} \int_{m_{\tilde{Z}_i}}^{E_{\max}} dE \frac{\sqrt{E^2 - m_{\tilde{Z}_i}^2}}{(m_{\tilde{W}_j}^2 + m_{\tilde{Z}_i}^2 - 2m_{\tilde{W}_j}E - M_W^2)^2}$$
$$\times \{(|X_j^i|^2 + |Y_j^i|^2)[3(m_{\tilde{W}_j}^2 + m_{\tilde{Z}_i}^2)m_{\tilde{W}_j}E$$
$$- 2m_{\tilde{W}_j}^2(2E^2 + m_{\tilde{Z}_i}^2)] - 3(|X_j^i|^2 - |Y_j^i|^2)$$
$$\times m_{\tilde{W}_j} m_{\tilde{Z}_i}(m_{\tilde{W}_j}^2 + m_{\tilde{Z}_i}^2 - 2Em_{\tilde{W}_j})\}. \quad \text{(A26)}$$

Here X_j^i and Y_j^i are the $W\tilde{W}_j\tilde{Z}_i$ couplings as defined in Ref. [18], and the upper integration limit $E_{\max}$ is given by Eq. (A14) with $m_{\tilde{Z}_j} \to m_{\tilde{W}_j}$ and $m_f \to 0$.

The *squared sneutrino exchange contribution* is given by

$$\Gamma_{\tilde{\nu}} = 2(\tilde{A}_{\tilde{Z}_i}^{\nu})^2[(\tilde{A}_{\tilde{W}_j}^{\tau})^2 + (B_{\tilde{W}_j}^{\tau})^2]^2 \psi(m_{\tilde{W}_j}, m_{\tilde{\nu}_\tau}, m_{\tilde{Z}_i}). \quad \text{(A27)}$$

The couplings appearing in Eq. (A27) have been defined in Eqs. (A2), and the kinematical function ψ is given in Ref. [21].

The *pure scalar tau exchange terms* can be written as

$$\Gamma_{\tilde{\tau}} = \Gamma_{\tilde{\tau}_1} + \Gamma_{\tilde{\tau}_2} + \Gamma_{\tilde{\tau}_1\tilde{\tau}_2}, \quad \text{(A28)}$$

where

$$\Gamma_{\tilde{\tau}_k} = 2(\alpha_{\tilde{W}_j}^{\tilde{\tau}_k})^2[(\alpha_{\tilde{Z}_i}^{\tilde{\tau}_k})^2 + (\beta_{\tilde{Z}_i}^{\tilde{\tau}_k})^2]\psi(m_{\tilde{W}_j}, m_{\tilde{\tau}_k}, m_{\tilde{Z}_i}), \quad \text{(A29a)}$$

$$\Gamma_{\tilde{\tau}_1\tilde{\tau}_2} = 4\alpha_{\tilde{W}_j}^{\tilde{\tau}_1}\alpha_{\tilde{W}_j}^{\tilde{\tau}_2}[\alpha_{\tilde{Z}_i}^{\tilde{\tau}_1}\alpha_{\tilde{Z}_i}^{\tilde{\tau}_2} + \beta_{\tilde{Z}_i}^{\tilde{\tau}_1}\beta_{\tilde{Z}_i}^{\tilde{\tau}_2}]\tilde{\psi}(m_{\tilde{W}_j}, m_{\tilde{\tau}_1}, m_{\tilde{\tau}_2}, m_{\tilde{Z}_i}). \quad \text{(A29b)}$$

The couplings appearing in Eqs. (A29) have been defined in Eqs. (A4)–(A7), and the functions ψ, $\tilde{\psi}$ are as defined above.

The *squared charged Higgs boson exchange contribution* is

$$\Gamma_H = \pi^2 m_{\tilde{W}_j}\left(\frac{g m_\tau \tan\beta}{M_W}\right)^2 \int_{m_{\tilde{Z}_i}}^{E_{\max}} dE \sqrt{E^2 - m_{\tilde{Z}_i}^2} \frac{(m_{\tilde{W}_j}^2 + m_{\tilde{Z}_i}^2 - 2E_{m\tilde{W}_j})\{E[(\alpha_{\tilde{W}_j}^{(i)})^2 + (\beta_{\tilde{W}_j}^{(i)})^2] + 2(-1)^{\theta_i+\theta_j} m_{\tilde{Z}_i}\alpha_{\tilde{W}_j}^{(i)}\beta_{\tilde{W}_j}^{(i)}\}}{(m_{\tilde{W}_j}^2 + m_{\tilde{Z}_i}^2 - 2Em_{\tilde{W}_j} - m_{H^+}^2)^2}. \quad \text{(A30)}$$

Here, $E_{\max}$ is the same as in Eq. (A26), the $H^+\tilde{W}_j^-\tilde{Z}_i$ couplings have been defined in Eqs. (A8), and $\theta_j (\equiv \theta_-$ or θ_+ in the notation of Ref. [18]$) = 0$ (1) if the corresponding eigenvalue of the chargino mass matrix is positive (negative).

The *W-sneutrino interference contribution* is not affected by $\tilde{\tau}_L$-$\tilde{\tau}_R$ mixing and contributions $\propto f_\tau$; it can be written as

$$\Gamma_{W\tilde{\nu}} = -4\sqrt{2}g^2(-1)^{\theta_i+\theta_j}\tilde{A}_{\tilde{W}_j}^{\tau}\tilde{A}_{\tilde{Z}_i}^{\nu}[(X_j^i - Y_j^i)I_1(m_{\tilde{W}_j}, m_{\tilde{\nu}_\tau}, m_{\tilde{Z}_i})$$
$$- (X_j^i + Y_j^i)I_2(m_{\tilde{W}_j}, m_{\tilde{\nu}_\tau}, m_{\tilde{Z}_i})], \quad \text{(A31)}$$

where we have introduced the functions

$$I_1(m_{\tilde{W}}, m_{\tilde{f}}, m_{\tilde{Z}}) = \frac{\pi^2}{2m_{\tilde{W}}} \int_0^{(m_{\tilde{W}} - m_{\tilde{Z}})^2} \frac{ds}{s - M_W^2}$$
$$\times \left[-\frac{1}{2} Q(m_{\tilde{W}}E_Q + m_{\tilde{f}}^2 - m_{\tilde{W}}^2 - s) \right.$$
$$\left. - \frac{(m_{\tilde{f}}^2 - m_{\tilde{Z}}^2)(m_{\tilde{f}}^2 - m_{\tilde{W}}^2)}{4m_{\tilde{W}}} \right.$$
$$\left. \times \log \frac{m_{\tilde{W}}(E_Q + Q) - \mu^2}{m_{\tilde{W}}(E_Q - Q) - \mu^2} \right], \quad \text{(A32a)}$$

$$I_2(m_{\tilde{W}}, m_{\tilde{f}}, m_{\tilde{Z}}) = \frac{\pi^2}{8m_{\tilde{W}}} \int_0^{(m_{\tilde{W}} - m_{\tilde{Z}})^2} \frac{ds}{s - M_W^2} m_{\tilde{Z}} s$$
$$\times \log \frac{m_{\tilde{W}}(E_Q + Q) - \mu^2}{m_{\tilde{W}}(E_Q - Q) - \mu^2}. \quad \text{(A32b)}$$

The quantities μ^2, E_Q, and Q are as in Eq. (A20), with $m_{\tilde{Z}_j} \to m_{\tilde{W}}$, $m_{\tilde{Z}_i} \to m_{\tilde{Z}}$ and $m_{\tilde{f}_k} \to m_{\tilde{f}}$.

The same functions also appear in the *W-scalar tau interference contributions*:

$$\Gamma_{W\tilde{\tau}} = \Gamma_{W\tilde{\tau}_1} + \Gamma_{W\tilde{\tau}_2}, \quad \text{(A33)}$$

where

$$\Gamma_{W\tilde{\tau}_k} = 4\sqrt{2}g^2\alpha_{\tilde{W}_j}^{\tilde{\tau}_k}\alpha_{\tilde{Z}_i}^{\tilde{\tau}_k}[(X_j^i + Y_j^i)I_1(m_{\tilde{W}_j}, m_{\tilde{\tau}_k}, m_{\tilde{Z}_i})$$
$$- (X_j^i - Y_j^i)I_2(m_{\tilde{W}_j}, m_{\tilde{\tau}_k}, m_{\tilde{Z}_i})]. \quad \text{(A34)}$$

The couplings X_j^i, Y_j^i can be found in Ref. [18]; the remaining couplings appearing in Eq. (A34) have been introduced in Eqs. (A4)–(A7).

The *sneutrino-scalar tau interference terms* can be written as

$$\Gamma_{\tilde{\nu}\tilde{\tau}} = \Gamma_{\tilde{\nu}\tilde{\tau}_1} + \Gamma_{\tilde{\nu}\tilde{\tau}_2}, \quad \text{(A35)}$$

where

$$\Gamma_{\tilde{\nu}\tilde{\tau}_k} = -4\tilde{A}^{\nu}_{\tilde{Z}_i}\alpha^{\tilde{\tau}_k}_{\tilde{W}_j}[B^{\tau}_{\tilde{W}_j}\beta^{\tilde{\tau}_k}_{\tilde{Z}_i}Y(m_{\tilde{W}_j},m_{\tilde{\nu}_\tau},m_{\tilde{\tau}_k},m_{\tilde{Z}_i}) - (-1)^{\theta_i+\theta_j}\tilde{A}^{\tau}_{\tilde{W}_j}\alpha^{\tilde{\tau}_k}_{\tilde{Z}_i}\tilde{\phi}(m_{\tilde{W}_j},m_{\tilde{\nu}_\tau},m_{\tilde{\tau}_k},m_{\tilde{Z}_i})]. \tag{A36}$$

The functions Y, $\tilde{\phi}$ have already been defined.

The *charged Higgs-sneutrino interference term* is given by

$$\Gamma_{H\tilde{\nu}} = 2\sqrt{2}\tilde{A}^{\nu}_{\tilde{Z}_i}B^{\tau}_{\tilde{W}_j}\frac{gm_\tau\tan\beta}{m_W}I_H(m_{\tilde{W}_j},m_{H^+},m_{\tilde{\nu}_\tau},m_{\tilde{Z}_i}), \tag{A37}$$

where we have introduced the function

$$I_H(m_{\tilde{W}_j},m_H,m_{\tilde{f}},m_{\tilde{Z}_i}) = \frac{\pi^2}{2m_{\tilde{W}_j}}\int_0^{(m_{\tilde{W}_j}-m_{\tilde{Z}_i})^2}\frac{ds}{s-m_H^2}\left\{\frac{1}{2}sQ\beta^{(i)}_{\tilde{W}_j} + \frac{1}{4m_{\tilde{W}_j}}[\beta^{(i)}_{\tilde{W}_j}sm_{\tilde{f}}^2+(-1)^{\theta_i+\theta_j}\alpha^{(i)}_{\tilde{W}_j}m_{\tilde{W}_j}m_{\tilde{Z}_i}s]\times\log\frac{m_{\tilde{W}_j}(E_Q+Q)-\mu^2}{m_{\tilde{W}_j}(E_Q-Q)-\mu^2}\right\}, \tag{A38}$$

the quantities μ^2, E_Q, and Q are as in Eq. (A20), with $m_{\tilde{Z}_j}\to m_{\tilde{W}_j}$. The charged Higgs couplings appearing in the integrand of Eq. (A38) have been defined in Eqs. (A8).

The same function also appears in the *charged Higgs-scalar tau interference contributions*:

$$\Gamma_{H\tilde{\tau}} = \Gamma_{H\tilde{\tau}_1}+\Gamma_{H\tilde{\tau}_2}, \tag{A39}$$

where

$$\Gamma_{H\tilde{\tau}_k} = 2\sqrt{2}\alpha^{\tilde{\tau}_k}_{\tilde{W}_j}\beta^{\tilde{\tau}_k}_{\tilde{Z}_i}\frac{gm_\tau\tan\beta}{M_W}I_H(m_{\tilde{W}_j},m_{H^+},m_{\tilde{\tau}_k},m_{\tilde{Z}_i}). \tag{A40}$$

The partial widths for the analogous neutralino to chargino decays are given by crossing:

$$\Gamma(\tilde{Z}_i\to\tilde{W}_j^+\tau^-\overline{\nu}_\tau) = \Gamma(\tilde{W}_j^-\to\tilde{Z}_i\tau^-\overline{\nu}_\tau)(m_{\tilde{W}_j}\leftrightarrow m_{\tilde{Z}_i}). \tag{A41}$$

Note that $\tilde{Z}_i$ can also decay into $\tilde{W}_j^-\tau^+\nu_\tau$ final states, with equal probability. However, these neutralino decays are usually not very important, since they are either phase space suppressed, or have to compete with two-body decays of the heavy neutralinos.

4. $\tilde{g}\to\tilde{W}_i t\overline{b}$ decays

These decays proceed through the exchange of any of the four top squark and sbottom mass eigenstates; in the limit θ_b, $f_b\to 0$ considered in the existing literature [21], only one of the two sbottom eigenstates contributes here, since $\tilde{b}_R$ does not couple to charginos in this limit. Fortunately the general case does not introduce terms with new Dirac structure in the matrix elements; the necessary phase space integrals can therefore be extracted from the Appendix of Ref. [21].

We begin by defining eight kinematical functions:

$$G_1(m_{\tilde{g}},m_{\tilde{t}},m_{\tilde{W}}) = m_{\tilde{g}}\int\frac{dE_t p_t E_t(m_{\tilde{g}}^2+m_t^2-2E_t m_{\tilde{g}}-m_{\tilde{W}}^2)^2}{(m_{\tilde{g}}^2+m_t^2-2E_t m_{\tilde{g}}-m_{\tilde{t}}^2)^2(m_{\tilde{g}}^2+m_t^2-2E_t m_{\tilde{g}})}, \tag{A42a}$$

$$G_2(m_{\tilde{g}},m_{\tilde{b}},m_{\tilde{W}}) = m_{\tilde{g}}\int dE_{\overline{b}}E_{\overline{b}}^2\lambda^{1/2}(m_{\tilde{g}}^2+m_b^2-2E_{\overline{b}}m_{\tilde{g}},m_{\tilde{W}}^2,m_t^2)\times\frac{m_{\tilde{g}}^2+m_b^2-m_t^2-2E_{\overline{b}}m_{\tilde{g}}-m_{\tilde{W}}^2}{(m_{\tilde{g}}^2+m_b^2-2E_{\overline{b}}m_{\tilde{g}}-m_{\tilde{b}}^2)^2(m_{\tilde{g}}^2+m_b^2-2E_{\overline{b}}m_{\tilde{g}})}, \tag{A42b}$$

$$G_3(m_{\tilde{g}},m_{\tilde{b}},m_{\tilde{W}}) = (-1)^{\theta_{\tilde{W}}}4m_{\tilde{g}}m_{\tilde{W}}m_t\int dE_{\overline{b}}E_{\overline{b}}^2\lambda^{1/2}(m_{\tilde{g}}^2+m_b^2-2E_{\overline{b}}m_{\tilde{g}},m_{\tilde{W}}^2,m_t^2)\times\frac{1}{(m_{\tilde{g}}^2+m_b^2-2E_{\overline{b}}m_{\tilde{g}}-m_{\tilde{b}}^2)^2(m_{\tilde{g}}^2+m_b^2-2E_{\overline{b}}m_{\tilde{g}})}, \tag{A42c}$$

$$G_4(m_{\tilde{g}},m_{\tilde{t}},m_{\tilde{b}},m_{\tilde{W}}) = (-1)^{\theta_{\tilde{g}}+\theta_{\tilde{W}}}m_{\tilde{g}}m_{\tilde{W}}\int\frac{dE_t}{m_{\tilde{g}}^2+m_t^2-2E_t m_{\tilde{g}}-m_t^2}\times\left[E_{\overline{b}}(\max)-E_{\overline{b}}(\min)-\frac{m_b^2+m_t^2-2E_t m_{\tilde{g}}-m_{\tilde{W}}^2}{2m_{\tilde{g}}}\log X\right], \tag{A42d}$$

$$G_5(m_{\tilde{g}},m_{\tilde{t}},m_{\tilde{b}},m_{\tilde{W}})=(-1)^{\theta_{\tilde{g}}}\frac{m_t}{2}\int dE_t\,\frac{m_{\tilde{g}}^2+m_t^2-2E_tm_{\tilde{g}}-m_{\tilde{W}}^2}{m_{\tilde{g}}^2+m_t^2-2E_tm_{\tilde{g}}-m_{\tilde{t}}^2}\log X, \tag{A42e}$$

$$G_6(m_{\tilde{g}},m_{\tilde{t}},m_{\tilde{b}},m_{\tilde{W}})=\frac{1}{2}\int\frac{dE_t}{m_{\tilde{g}}^2+m_t^2-2E_tm_{\tilde{g}}-m_{\tilde{t}}^2}\left\{\left[m_{\tilde{g}}(m_{\tilde{g}}^2+m_t^2-2E_tm_{\tilde{g}}-m_{\tilde{W}}^2)-\frac{m_{\tilde{b}}^2-m_{\tilde{g}}^2}{m_{\tilde{g}}}(2E_tm_{\tilde{g}}-m_t^2-m_{\tilde{g}}^2)\right]\log X\right.$$
$$\left.+2(2E_tm_{\tilde{g}}-m_t^2-m_{\tilde{g}}^2)[E_{\bar{b}}(\max)-E_{\bar{b}}(\min)]\right\}, \tag{A42f}$$

$$G_7(m_{\tilde{g}},m_{\tilde{t}},m_{\tilde{b}},m_{\tilde{W}})=(-1)^{\theta_{\tilde{W}}}\frac{1}{2}m_{\tilde{W}}m_t\int\frac{dE_t}{m_{\tilde{g}}^2+m_t^2-2E_tm_{\tilde{g}}-m_{\tilde{t}}^2}\left\{2[E_{\bar{b}}(\max)-E_{\bar{b}}(\min)]-\frac{m_{\tilde{b}}^2-m_{\tilde{g}}^2}{m_{\tilde{g}}}\log X\right\}, \tag{A42g}$$

$$G_8(m_{\tilde{g}},m_{\tilde{t}_1},m_{\tilde{t}_2},m_{\tilde{W}})=(-1)^{\theta_{\tilde{g}}}m_tm_{\tilde{g}}\int dE_t\,\frac{(m_{\tilde{g}}^2+m_t^2-2E_tm_{\tilde{g}}-m_{\tilde{W}}^2)[E_{\bar{b}}(\max)-E_{\bar{b}}(\min)]}{(m_{\tilde{g}}^2+m_t^2-2E_tm_{\tilde{g}}-m_{\tilde{t}_1}^2)(m_{\tilde{g}}^2+m_t^2-2E_tm_{\tilde{g}}-m_{\tilde{t}_2}^2)}. \tag{A42h}$$

Here, $\theta_{\tilde{g}}=0$ (1) if a positive (negative) gluino mass parameter is chosen, and $\theta_{\tilde{W}}$ ($=\theta_-$ or θ_+ in the notation of Ref. [18]) is the corresponding quantity for the chargino mass eigenstate. Further, we have introduced $E_{\bar{b}}(\min,\ \max)$ [21], which are given by

$$\frac{(m_{\tilde{g}}^2+m_t^2-2m_{\tilde{g}}E_t+m_b^2-m_{\tilde{W}}^2)(m_{\tilde{g}}-E_t)\mp p_t\lambda^{1/2}(m_{\tilde{g}}^2+m_t^2-2m_{\tilde{g}}E_t,m_b^2,m_{\tilde{W}}^2)}{2(m_{\tilde{g}}^2+m_t^2-2E_tm_{\tilde{g}})}. \tag{A43}$$

Also,

$$p_t=\sqrt{E_t^2-m_t^2} \tag{A44a}$$

and

$$X=\frac{m_{\tilde{b}}^2+2E_{\bar{b}}(\max)m_{\tilde{g}}-m_{\tilde{g}}^2}{m_{\tilde{b}}^2+2E_{\bar{b}}(\min)m_{\tilde{g}}-m_{\tilde{g}}^2}. \tag{A44b}$$

Finally, the limits of integration over E_t in Eqs. (A42) are from m_t to $(m_{\tilde{g}}^2+m_t^2-(m_{\tilde{W}}+m_b)^2)/2m_{\tilde{g}}$, while the integration over $E_{\bar{b}}$ in Eqs. (A42b) and (A42c) goes from m_b to $[m_{\tilde{g}}^2-(m_t+m_{\tilde{W}})^2]/2m_{\tilde{g}}$.

The partial widths for the processes under consideration can be written as

$$\Gamma(\tilde{g}\to t\bar{b}\tilde{W}_i)=\frac{1}{(2\pi)^2}\frac{1}{2m_{\tilde{g}}}\pi^2g_s^2$$
$$\times\left(\Gamma_{\tilde{t}_1}+\Gamma_{\tilde{t}_2}+\Gamma_{\tilde{t}_1\tilde{t}_2}+\Gamma_{\tilde{b}_1}+\Gamma_{\tilde{b}_2}+\sum_{k,l=1}^{2}\Gamma_{\tilde{t}_k\tilde{b}_l}\right), \tag{A45}$$

where g_s is the $SU(3)_c$ gauge coupling. Note that in the limit $m_b\to 0$ the two sbottom exchange diagrams do not interfere with each other. The individual contributions in Eq. (A45) are given by

$$\Gamma_{\tilde{t}_k}=[(\alpha_{\tilde{W}_i}^{\tilde{t}_k})^2+(\beta_{\tilde{W}_i}^{\tilde{t}_k})^2][G_1(m_{\tilde{g}},m_{\tilde{t}_k},m_{\tilde{W}_i})-(-1)^k\sin(2\theta_t)G_8(m_{\tilde{g}},m_{\tilde{t}_k},m_{\tilde{t}_k},m_{\tilde{W}_i})], \tag{A46a}$$

$$\Gamma_{\tilde{t}_1\tilde{t}_2}=-2(\alpha_{\tilde{W}_i}^{\tilde{t}_1}\alpha_{\tilde{W}_i}^{\tilde{t}_2}+\beta_{\tilde{W}_i}^{\tilde{t}_1}\beta_{\tilde{W}_i}^{\tilde{t}_2})\cos(2\theta_t)G_8(m_{\tilde{g}},m_{\tilde{t}_1},m_{\tilde{t}_2},m_{\tilde{W}_i}), \tag{A46b}$$

$$\Gamma_{\tilde{b}_k}=[(\alpha_{\tilde{W}_i}^{\tilde{b}_k})^2+(\beta_{\tilde{W}_i}^{\tilde{b}_k})^2]G_2(m_{\tilde{g}},m_{\tilde{b}_k},m_{\tilde{W}_i})-\alpha_{\tilde{W}_i}^{\tilde{b}_k}\beta_{\tilde{W}_i}^{\tilde{b}_k}G_3(m_{\tilde{g}},m_{\tilde{b}_k},m_{\tilde{W}_i}), \tag{A46c}$$

$$\Gamma_{\tilde{t}_1\tilde{b}_1} = (\cos\theta_t \sin\theta_b \alpha^{\tilde{b}_1}_{\tilde{W}_i}\beta^{\tilde{t}_1}_{\tilde{W}_i} + \sin\theta_t \cos\theta_b \beta^{\tilde{b}_1}_{\tilde{W}_i}\alpha^{\tilde{t}_1}_{\tilde{W}_i}) G_6(m_{\tilde{g}}, m_{\tilde{t}_1}, m_{\tilde{b}_1}, m_{\tilde{W}_i})$$
$$-(\cos\theta_t \cos\theta_b \alpha^{\tilde{b}_1}_{\tilde{W}_i}\alpha^{\tilde{t}_1}_{\tilde{W}_i} + \sin\theta_t \sin\theta_b \beta^{\tilde{b}_1}_{\tilde{W}_i}\beta^{\tilde{t}_1}_{\tilde{W}_i}) G_4(m_{\tilde{g}}, m_{\tilde{t}_1}, m_{\tilde{b}_1}, m_{\tilde{W}_i})$$
$$+(\cos\theta_t \cos\theta_b \beta^{\tilde{b}_1}_{\tilde{W}_i}\alpha^{\tilde{t}_1}_{\tilde{W}_i} + \sin\theta_t \sin\theta_b \alpha^{\tilde{b}_1}_{\tilde{W}_i}\beta^{\tilde{t}_1}_{\tilde{W}_i}) G_5(m_{\tilde{g}}, m_{\tilde{t}_1}, m_{\tilde{b}_1}, m_{\tilde{W}_i})$$
$$-(\cos\theta_t \sin\theta_b \beta^{\tilde{b}_1}_{\tilde{W}_i}\beta^{\tilde{t}_1}_{\tilde{W}_i} + \sin\theta_t \cos\theta_b \alpha^{\tilde{b}_1}_{\tilde{W}_i}\alpha^{\tilde{t}_1}_{\tilde{W}_i}) G_7(m_{\tilde{g}}, m_{\tilde{t}_1}, m_{\tilde{b}_1}, m_{\tilde{W}_i}). \quad \text{(A46d)}$$

The couplings appearing in Eqs. (A46) are listed in Eqs. (A4)–(A7). The other top-squark–sbottom interference contributions can be obtained from Eq. (A46d) by substituting the appropriate coupling constants and squark masses; in addition, one has to apply the substitution rules (A6) to the factors in Eq. (A46d) that depend on third generation squark mixing angles. Finally, we note that gluinos have the same partial widths for decays into $t\bar{b}\tilde{W}_i^-$ and $\bar{t}b\tilde{W}_i^+$ final states.

These formulas have been incorporated into the event generator ISAJET 7.32 [9]. Finally, we remark that we have also updated the formula for $\Gamma(\tilde{g}\to t\bar{t}\tilde{Z}_i)$ that appears in Ref. [21] to include $\tilde{t}_L-\tilde{t}_R$ mixing effects. This has also been incorporated into ISAJET.

[1] A. Chamseddine, R. Arnowitt, and P. Nath, Phys. Rev. Lett. **49**, 970 (1982); R. Barbieri, S. Ferrara, and C. Savoy, Phys. Lett. **119B**, 343 (1982); L. J. Hall, J. Lykken, and S. Weinberg, Phys. Rev. D **27**, 2359 (1983); for a review, see H. P. Nilles, Phys. Rep. **110**, 1 (1984).

[2] For recent reviews, see X. Tata, *Lectures Presented at the IX Jorge Swieca Summer School*, Campos do Jordão, Brazil, February 1997, Report No. UH-511-872-97, hep-ph/9706307; S. Dawson, Lectures at *TASI 97*, hep-ph/9712464, 1997.

[3] H. Baer, M. Bhrlik, R. Munroe, and X. Tata, Phys. Rev. D **52**, 5031 (1995).

[4] H. Baer, C-H. Chen, C. Kao, and X. Tata, Phys. Rev. D **52**, 1565 (1995); H. Baer, C-H. Chen, F. Paige, and X. Tata, *ibid.* **54**, 5866 (1996).

[5] T. Kamon, J. Lopez, P. McIntyre, and J. T. White, Phys. Rev. D **50**, 5676 (1994); S. Mrenna, G. Kane, G. D. Kribs, and J. D. Wells, *ibid.* **53**, 1168 (1996).

[6] ATLAS Collaboration, technical proposal, Report No. CERN/LHCC 94-43, 1994; CMS Collaboration, technical proposal, Report No. CERN/LHCC 94-38; H. Baer, C-H. Chen, F. Paige, and X. Tata, Phys. Rev. D **52**, 2746 (1995); **53**, 6241 (1996); A. Bartl *et al.*, in *New Directions for High Energy Physics*, edited by D. Cassel, L. Trindle Gennari, and R. Siemann, 1997 (unpublished), p. 693; I. Hinchliffe *et al.*, Phys. Rev. D **55**, 5520 (1997).

[7] T. Tsukamoto, K. Fujii, H. Murayama, M. Yamaguchi, and Y. Okada, Phys. Rev. D **51**, 3153 (1995); H. Baer, R. Munroe, and X. Tata, *ibid.* **54**, 6735 (1996); A. Bartl, H. Eberl, S. Kraml, W. Majerotto, W. Porod, and A. Sopczak, Z. Phys. C **76**, 549 (1997).

[8] M. Nojiri, K. Fujii, and T. Tsukamoto, Phys. Rev. D **54**, 6756 (1996).

[9] F. Paige and S. Protopopescu, in *Supercollider Physics*, edited by D. Soper (World Scientific, Singapore, 1986), p. 41; H. Baer, F. Paige, S. Protopopescu, and X. Tata, in *Proceedings of the Workshop on Physics at Current Accelerators and Supercolliders*, edited by J. Hewett, A. White, and D. Zeppenfeld, Argonne National Laboratory, 1993, hep-ph/9305342.

[10] M. Drees and M. Nojiri, Nucl. Phys. **B369**, 54 (1992).

[11] H. Baer, C-H. Chen, M. Drees, F. Paige, and X. Tata, Phys. Rev. Lett. **79**, 986 (1997).

[12] M. Carena, J. Espinosa, M. Quiros, and C. Wagner, Phys. Lett. B **355**, 209 (1995); M. Carena, M. Quiros, and C. E. M. Wagner, Nucl. Phys. **B461**, 407 (1996); H. Haber, R. Hempfling, and A. Hoang, Z. Phys. C **75**, 539 (1997).

[13] M. Bisset, Ph.D. thesis, Hawaii Report No. UH-511-813-94, 1994.

[14] A. Bartl, W. Majerotto, and W. Porod, Z. Phys. C **64**, 499 (1994); **68**, 518(E) (1995).

[15] H. Baer, K. Hagiwara, and X. Tata, Phys. Rev. D **35**, 1598 (1987); R. Arnowitt and P. Nath, Mod. Phys. Lett. A **2**, 331 (1987); H. Baer and X. Tata, Phys. Rev. D **47**, 2739 (1993); H. Baer, C. Kao, and X. Tata, *ibid.* **48**, 5175 (1993); S. Mrenna, G. Kane, G. D. Kribs, and J. D. Wells, *ibid.* **53**, 1168 (1996); see also Ref. [4].

[16] M. Hohlmann, Report No. Fermilab-Conf-96/330-E, 1996.

[17] See e.g., ALEPH Collaboration, R. Barate *et al.*, Eur. J. Phys. **C2**, 417 (1998).

[18] H. Baer, V. Barger, D. Karatas, and X. Tata, Phys. Rev. D **36**, 96 (1987).

[19] H. Baer, X. Tata, and J. Woodside, Phys. Rev. D **42**, 1568 (1990).

[20] H. Baer, A. Bartl, D. Karatas, W. Majerotto, and X. Tata, Int. J. Mod. Phys. A **4**, 4111 (1989).

[21] H. Baer, X. Tata, and J. Woodside, Phys. Rev. D **45**, 142 (1992).

[22] M. Drees, C. S. Kim, and X. Tata, Phys. Rev. D **37**, 784 (1988).

[23] X. Tata and D. Dicus, Phys. Rev. D **35**, 2110 (1987).